Application of Nickel Foam in Electrochemical Systems: A Review

Mpho S. Ratsoma[1], Boipelo L.O. Poho[1], Katlego Makgopa[1*], Kumar Raju[2], Kwena D. Modibane[3], Charl J. Jafta[4], and Kabir O. Oyedotun[5*]

[1] Department of Chemistry, Faculty of Science, Tshwane University of Technology (Arcadia Campus), Pretoria 0001, South Africa
[2] Institute for Manufacturing, University of Cambridge, Cambridge CB3 0FS, United Kingdom
[3] Department of Chemistry, School of Physical and Mineral Sciences, University of Limpopo (Turfloop), Sovenga 0727, Polokwane, South Africa
[4] Electrification and Energy Infrastructure Division, Oak Ridge National Laboratory, Oak Ridge, TN, 37830, United State of America
[5] Department of Physics, Institute of Applied Materials, SARChI Chair in Carbon Technology and Materials, University of Pretoria, Pretoria 0028, South Africa.

**Corresponding authors' emails: MakgopaK@tut.ac.za; kabir.oyedotun@gmail.com.*

Abstract

The effectiveness of electrochemical systems in various applications (e.g., energy storage and conversion, waste-water treatment, ammonia synthesis, etc.) is in essence, dependent on the electrode materials employed in such systems. Research emphasis on such electrochemical systems is given to developing electrode materials that would offer cost-effectiveness, stability, and reliable results that can be practical for commercial scaling. However, the operation of such systems also relies on other various components that include electrode fabrication, electrolytes, system architecture, the durability of the systems, and supporting components (i.e., substrate/ current collector). On the choice of the current collector, nickel foam (NF) has enjoyed a widespread attention as a favorable substrate in various electrochemical systems. This growing trend is attributed to its unique interlinked three-dimensional (3D) structure that offers advantages such as lightweight, high porosity, great mechanical strength, chemical stability, and encouraging electrical and thermal conductivity. These traits are favorable for maximized contact areas between the current collector, the active materials, and charged species resulting in the reduction of charge transport pathways, which is a vital step for improving the electrochemical performance. This review aims at highlighting the use of NF as a substrate of choice in developing effective electrodes for various electrochemical systems and act as a navigational tool to the literature involving the use of NF as the current collector. It also shows to a certain extent, the impact of NF on the electrochemical performance as compared to other current collectors.

Keywords: Nickel foam; Three-dimensional structure; Electrochemical systems; Energy storage; Electrocatalyst.

Table of Contents

1. Introduction

Electrochemical systems have become an integral part of modern society as they have found immense application in various vital aspects of everyday human life such as in medicine and healthcare, energy storage and conversion, waste-water treatment, environmental monitoring and remediation, industry, etc. The overall practical effectiveness of electrochemical systems largely depends on the efficacy of their electrodes toward the intended operations. However, the efficiency of the electrode is in itself dependent on the components making up the electrode, as well as the design of the electrode. The electrodes of an electrochemical system include a current collector connected to an external wire, and additive conductive, binding, and active materials.[1–4] The role of current collectors is to link the active material to the external circuit for the flow of electrons between terminals (i.e., cathode and anode). The ideal current collectors exhibit properties such as good electrical and thermal conductivity, chemical and thermal stability, and high surface area (per mass or volume ratio). Current collectors employed in various electrochemical systems include metal foams (e.g. Ni, Al, Fe, etc.), metal sheets (Pt, Ti, Cu, etc.), carbon cloth, non-stick tape, stainless steel, etc.[1]

Amongst various current collectors, metal foams attract attention since they also offer an effective shape to the electrode as a result of their interlinked three-dimensional (3D) structure in addition to providing a powerful link between the active material and the external circuit.[5,6] Nickel foam (NF) in particular has found immeasurable favor for use as a current collector in various electrochemical applications due to it being exceptionally uniform, highly porous, and lightweight (Fig. 1). Additionally, NF displays favorable properties such as great mechanical strength, encouraging electrical and thermal conductivity, small ionic diffusion resistance, good corrosion resistance, and increased areal loading of active materials.[6–9] The exploitation of some of these properties results in highly stable electrodes with maximized contact areas between the NF, the active materials, and charged species which is beneficial for improved electrochemical performance. Hence, NF has been used as a current collector in various electrochemical systems such as energy storage (i.e., electrochemical capacitors and rechargeable batteries) and conversion (i.e., fuel cells and water splitting), chemical sensors, wastewater treatment, ammonia production, etc. [1,10]

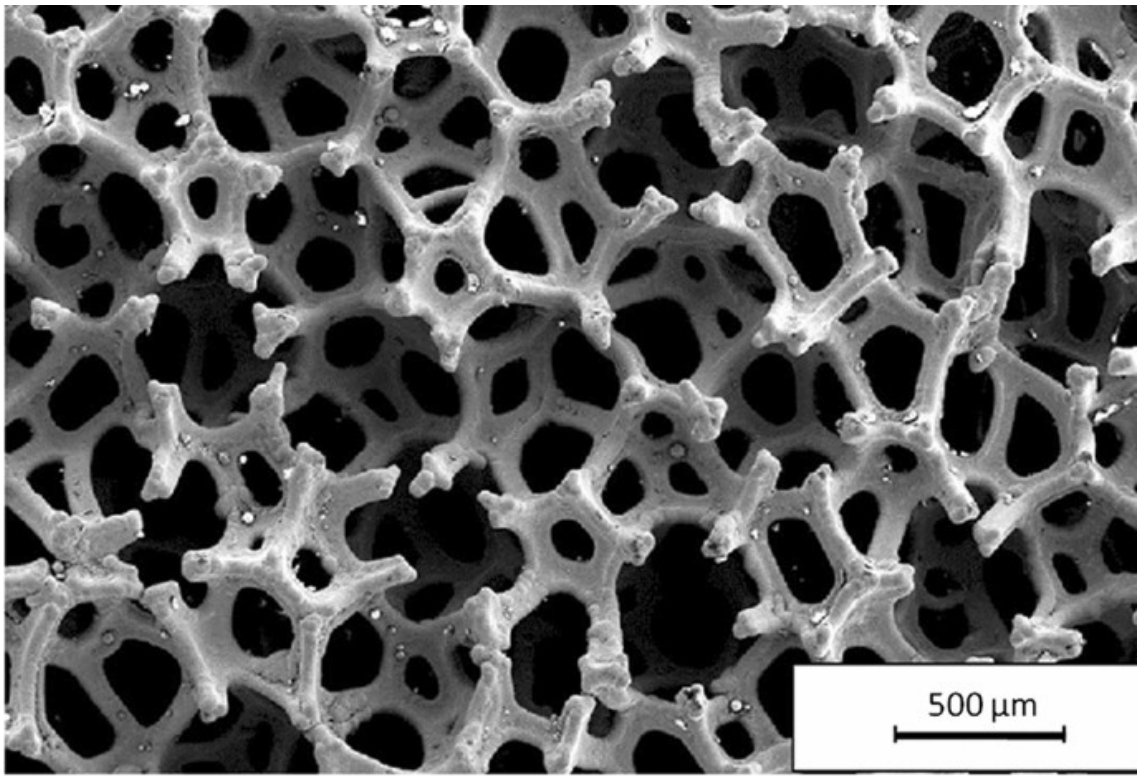

Figure 1: *The structure of nickel foam (NF). Reprinted with permission from Ref.* [14]*. Copyright 2019, Springer Nature.*

As much as NF has enjoyed a fair amount of application in electrochemical systems, it is worth noting that some researchers argued the use of NF as the current collector as it is said to lead to exaggerated electrochemical performance due to the electrochemical activity observed from bare NF.[11] Nevertheless, based on the volume of reported studies in the literature, NF has continued to be the material of choice as current collector in various electrochemical systems.[12,13] Hence the focus of this review is to highlight the use of NF as a current collector of choice in various electrochemical systems, while also highlighting to a certain extent the impact of NF on the electrochemical performance compared to other current collectors. The review also aims to serve as a directory collection of literature involving the use of NF for an audience interested in using it as a current collector.

2. Nickel foam as a current collector: Uncertainties

As mentioned above, there is substantial growth in the literature reporting the use of NF as a current collector of choice in various electrochemical applications. Nonetheless, some researchers have expressed concerns about the role that NF is perceived to play in the overall performance of the electrode. For instance, Xing et al[11] questioned the validity of the results reported in studies that employed NF as a current collector in electrochemical capacitors (ECs), suggesting that NF is electrochemically active and leads to erroneous and exaggerated electrochemical measurements. They conducted comparative studies on mesoporous carbon and mesoporous nickel oxide using NF and titanium (Ti) gauze as current collectors to illustrate their argument on the impact NF current collector has on the electrochemical performance. The NF results displayed higher electrochemical performance (i.e., C_{sp} of 190 F g^{-1} for mesoporous carbon and 494 F g^{-1} for NiO) as compared to those of Ti gauze (i.e., C_{sp} of 22 F g^{-1} for mesoporous carbon and 129 F g^{-1} for NiO). They attributed this observation to the presence of electrochemically active nickel hydroxides/ oxides that remain on bare NF even after pre-treatment. Hence, in their observation, the NF-supported active materials displayed much higher electrochemical performance compared to the Ti gauze-supported materials. In another study, Geaney et al[15] demonstrated the electrochemical contribution of high-temperature (between 300 – 450 °C) treated NF current collector to the specific capacity in lithium-ion batteries. Their investigation revealed that the bare-NF heated at 300 °C and 450 °C displayed slightly higher charge capacities of ~0.3 and ~1.3 mAh, respectively. They attributed this observation to the formation of an oxide layer on the surface of NF. Further analysis of NF pretreated at 450 °C and decorated with Co_3O_4 nanoflowers showed an improved capacity of ~2.7 mAh (with ~48% of the capacity originating from the oxide layer of NF, assuming similar mass loading of the oxide layer on both the bare and Co_3O_4 decorated NF). However, it is worth mentioning that the investigation also showed a negligible contribution of NF (i.e., pristine and pretreated at ≤ 100 °C) to the overall electrochemical performance.

Because of the above-mentioned uncertainties, some researchers have opted to use electrochemically inert materials to coat one side of NF-based electrodes to limit or avoid any potential activity that may occur on the surface of NF while making measurements on the active materials-coated side of the NF.[16] Conversely, many literature reports involving NF as a current collector, use control tests as means of probing the impact of NF on the overall electrochemical performance and have demonstrated that the contribution of NF is often negligible compared

to the electrochemical activity of the active material.[17–19] The next section highlights the use of NF as a substrate of choice in developing effective electrodes in various electrochemical systems such as energy storage (i.e., electrochemical capacitors and rechargeable batteries) and conversion (i.e., fuel cells and water splitting), chemical sensors, wastewater treatment, ammonia production.

3. Electrochemical Applications

3.1. Energy Storage and Conversion

3.1.1. Electrochemical Capacitors

Over the past two decades, electrochemical capacitors (ECs), also known as ultracapacitors (UCs) or supercapacitors (SCs), have drawn great interest as power sources for applications requiring quick bursts of energy (fast discharge), such as high-power electronic devices, electric vehicles, uninterrupted power supply (UPS), as well as serving as a backup to batteries.[20–22] The high energy and power performance disposition of SCs give them a key role in bridging the gap between batteries and electrolytic capacitors, as they can deliver more power with better cycling than batteries while storing more energy than traditional capacitors.[23] Generally, ECs are classified into three categories that are based on their charge storage mechanism: (i) electrical double-layer capacitors (EDLCs) that involve reversible ion adsorption on electrically charged surfaces and (ii) pseudocapacitors (PCs) that involve fast surface redox reactions on the surface of the electroactive materials, and hybrid supercapacitors that incorporate the electrostatic mechanism of the EDLCs with the 'sluggish" redox reactions of battery-type electrode materials.[24,25] The performance of ECs relies on the chemical and morphological properties (i.e., size, shape, surface area, and architecture) of the electrode materials.[2,26] Hence, tremendous attention has been dedicated to the design and development of the EC electrode materials.[27–29]

The distinct electrochemical performance of NF as a current collector compared to other current collectors was evidenced by, amongst others, Makgopa et al[10] where NF was compared to platinum (Pt) disc as substrates for MnO_2/OLC nanohybrid electrode material for ECs applications. As shown in Fig. 2, the nanohybrid displayed a C_{sp} value of 295 F g^{-1} when supported on a Pt disc and 323 F g^{-1} on NF. Furthermore, the NF-supported electrode displayed a higher power density than the Pt disc counterpart. Zhang et al[30] managed to synthesize complex 3D graphene/cobalt sulfide on NF to produce NF/graphene/Co_3S_4 (NF/G/CS)

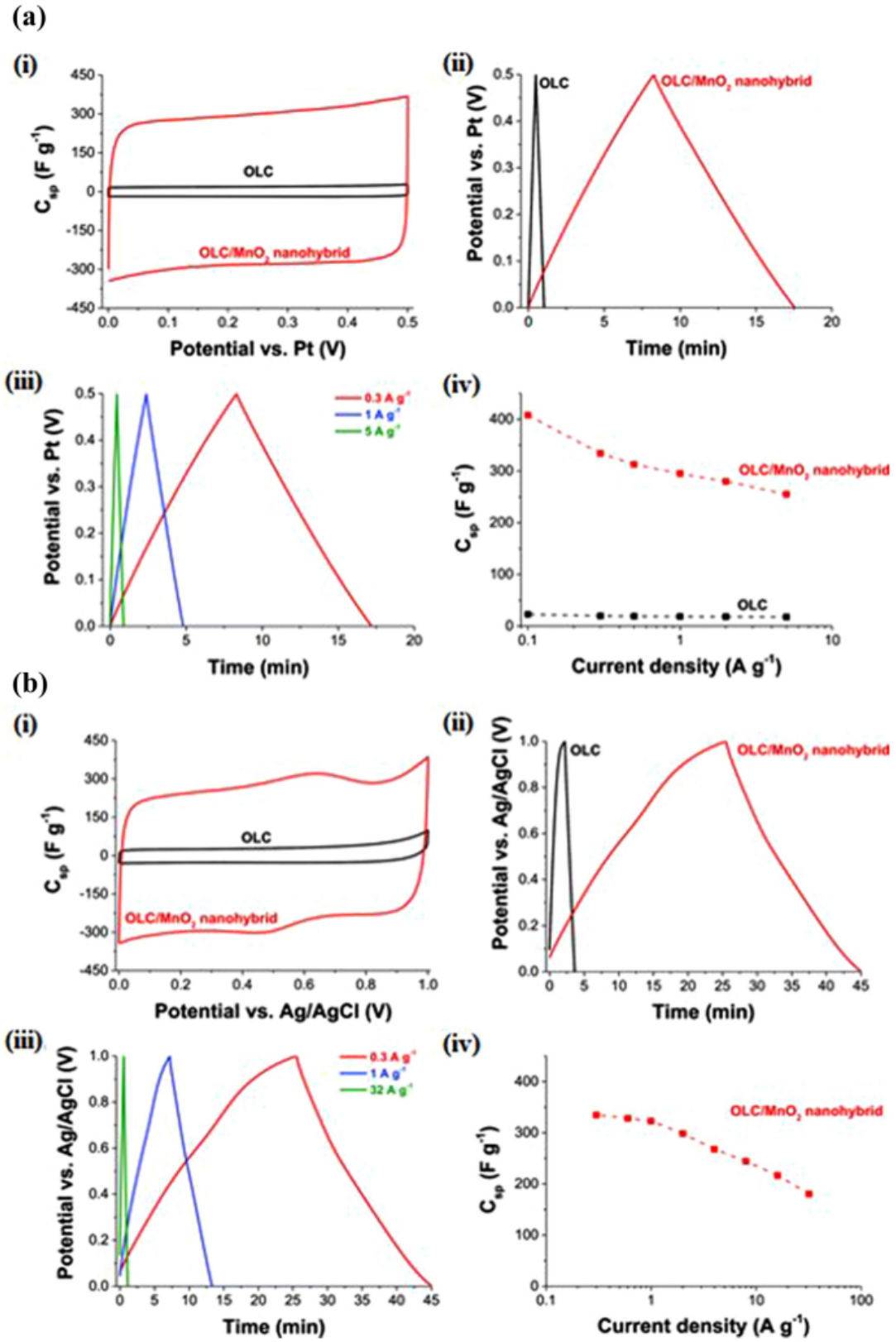

Figure 2: *Comparative electrochemical performance in a 3-electrode test with (A) Pt-disc and (B) Nickel foam as the current collectors. Reprinted (adapted) from Ref.* [10]*, with permission from the Royal Society of Chemistry under the terms of the Creative Commons CC BY license.*

nanocomposite that displayed outstanding electrochemical performance (i.e., areal capacitance (C_a) of 525 mF cm^{-2} at 7.5 mA cm^{-2}). The nanocomposite also displayed superior cycle stability (8 000 cycles) with a capacitance retention of 97.8%. The authors credited the results to the synergistic effects between the high surface area of hollow-like Co_3S_4 nanospheres, the excellent electronic and chemical properties of graphene, and the high mechanical strength of NF.

Jiang et al[31] synthesized Ni_3Se_2 nanosheets on the surface of NF via a one-step hydrothermal method that involved SeO_2 as a source of selenide (Se), and NF as a source of nickel (Ni). An asymmetric supercapacitor (ASC) set-up with activated carbon (AC) and Ni_3Se_2 showed potential stability for up to 1.6 V in a 3 M KOH electrolyte. The device displayed a specific energy density (E_{sp}) of 23.3 Wh kg^{-1} with a corresponding power density (P_d) of 398.1 W kg^{-1}, as well as great cycling stability of 91.11% capacitance retention after 5 000. The results obtained from the Ni_3Se_2/NF electrode were ascribed to the pseudocapacitive Ni_3Se_2 complex and the 3D structure of NF. Table 1 summarises reported literature that involved the use of NF as current collector for EC applications. Table 2 compares the electrochemical performance of NF-based electrodes with that of other current collectors, taking $NiCo_2O_4$ nanoparticles as common active material.

Table 1: *Summary of 3D NF-based electrode materials and their electrochemical performances in EC application.*

Electrode	Electrolyte	Device Set-up	C_{sp} (F g^{-1})	E_{sp} (Wh kg^{-1})	P_{max} (kW kg^{-1})	Ref.
Co_3O_4 nanowires	6 M KOH	Half-cell	1 160	-	-	[32]
$NiCo_2O_4$	3 M KOH	Half-cell	2 010	-	-	[33]
Graphene aerogel	6 M KOH	Half-cell	366	-	-	[34]
rGO	1 M Na_2SO_4	Half-cell	82.0	-	-	[35]
Graphene	6 M KOH	Half-cell	22.0	-	-	[36]
N-rGO/Mn_3O_4	1 M Na_2SO_4	Symmetric	345	12.0	22.5	[29]
$NH_4(NiCo)PO_4 \cdot H_2O$/GF	1 M KOH	Asymmetric	-	47.0	0.468	[37]
Pd-rGO/MOF	3 M KOH	Asymmetric	-	26.0	1.6	[38]
NF-rGO/MOF	3 M KOH	Asymmetric	(48.81 C g^{-1})[a]	11.0	0.640	[27]

$NH_4MnPO_4.H_2O$	3 M KOH	Asymmetric	65.4	29.4	133	[36]
$NiCo_2O_4@MnO_2$	1 M LiOH	Half-cell	1 471	-	-	[39]
$NiMoO_4$ NWs	2 M KOH	Half-cell	2 083	-	-	[40]
Ni-Al LDH	1 M KOH	Half-cell	795	-	-	[41]
$NiCo_2S_4$ nanotube arrays	6 M KOH	Half-cell	2 398	31.5	2.35	[42]
$MoSe_2$/Graphene	6 M KOH	Half-cell	1 422	-	-	[43]
$CuCo_2O_4@MnO_2$	1 M Na_2SO_4	Asymmetric	78	43.3	-	[44]
$NiCoO_2$	1 M KOH	Asymmetric	82	25.7	1.5	[45]
$Ni_xZn_{1-x}S$	3 M KOH	Asymmetric	127.7	38.9	0.33	[46]
OLC/Mn_3O_4	1 M Na_2SO_4	Asymmetric	-	19	45	[47]
Ni-Co-Mn oxide nanoflakes	(6:0.01 M) $KOH/K_3Fe(CN)_6$	Symmetric	298	41.4	5.4	[48]
Co_3O_4 nanoflakes	2 M KOH	Half-cell	(576.8 C g^{-1})[a]	-	-	[49]
$CuCo_2S_4$ nanograss	KOH/PVA	Symmetric	81.2	31.88	16.5	[50]
Ni_3S_2/Ni-Graphene foam	3 M KOH	Symmetric	190.5	67.7	2.66	[51]
Mo:ZnO	3 M KOH	Asymmetric	123	39.06	7.43	[52]
$CoNiSe_2$ nanorods	3 M KOH	Asymmetric	-	50.66	160	[53]
rGO/MnO_2	1 M Na_2SO_4	Symmetric	189	26.82	8.61	[54]
Ni_3S_2/NiV-LDH/rGO	2 M KOH	Asymmetric	147.9	59.4	10	[55]
$ZnCo_2O_4@CoMoO_4$	2 M KOH	Asymmetric	82.24	29.24	10.53	[56]
$NiMoO_4$-$CoMoO_4$	3 M KOH	Asymmetric	104.1	27.58	5.677	[57]
$Ni_3(NO_3)_2(OH)_4$	3 M KOH	Asymmetric	94.3	31.5	7.75	[58]
Ni_3S_2/3D G/NF	6 M KOH	Half-cell	2 565	-	-	[59]
$MgCo_2O_4@CoFe$	PVA/KOH	Asymmetric	208.3	60.82	3.625	[60]
NiCo-LDH	6 MKOH	Asymmetric	(131.3 C g^{-1})[a]	48.34	7.999	[61]

[a] Specific capacity (C g^{-1}, Ah g^{-1})

Table 2: *Comparative electrochemical performance of $NiCo_2O_4$ nanoparticles in EC applications using NF and other current collectors.*

Current Collector	Electrolyte	C_{sp} (F g^{-1})	Current Density (A g^{-1})	Ref.
Graphene foam	6 M KOH	1 402	1.0	[62]
Carbon cloth	2 M KOH	1 055	(2.5 mA cm^{-2})[a]	[63]
Graphite Rod	1 M Na_2SO_4	1 196	12.0	[64]
Stainless Steel	1 M KOH	1 027	1.0	[65]
FTO glass[d]	2 M KOH	1 073	(5.0 mA cm^{-2})[a]	[65]
NF	6 M KOH	1 797	1.0	[66]
Ni wire	2 M KOH	(315 C g^{-1})[b]	1.0	[67]
NF	2 M KOH	(670 C g^{-1})[b]	0.5	[68]
Carbon cloth	6 M KOH	(1 183 mF cm^{-2})[c]	(1.0 mA cm^{-2})[a]	[69]
Ni foil	6 M KOH	(1 139 mF cm^{-2})[b]	(1.0 mA cm^{-2})[a]	[70]
NF	2 M KOH	(3 510 mF cm^{-2})[b]	(1.8 mA cm^{-2})[a]	[71]

[a] Areal current density (A cm^{-2}); [b] Specific capacity (C g^{-1}, Ah g^{-1}); [c] Areal capacitance (F cm^{-2}); [D] FTO = Fluorine-tin oxide

3.1.2. Batteries

Rechargeable or secondary batteries have been demonstrated to be efficient technologies that can generate clean electricity recurrently by conversion of chemical energy via reversible redox reactions at the anode and cathode.[72] An ideal battery should possess desirable properties that include long life, small size, lightweight, high energy density, safety, environmental compatibility, low cost, and worldwide consumer distribution. Rechargeable batteries have found application as power sources in commercial sectors that include portable electronics, electric vehicles, and electricity grids. The energy storage qualities of batteries depend on both the performance of the active electrode materials and the integration technologies of battery components such as the electrolyte, electrode fabrication, build of the system, supporting components, and the durability of the systems.[73]

Sa and Wang compared copper (Cu) foil and NF as current collectors for high-capacity C–Si composite anode for lithium-ion batteries (LIB).[74] It was found, through a detailed comparison of the two current collectors, that the network geometry of NF displayed an improved cycle life for the silicon-based anode. The authors noted that the NF scaffold was able to support a larger weight percentage of silicon, which consequently bolstered the electrochemical efficiency of the LIB. The NF-supported Si-based anode possessed the smallest impedance, which is attributed to be an important aspect of the NF current collector. It was concluded in the study that the adoption of the 3D current collector provides a new way to incorporate electrode materials experiencing large expansion in volume.

Feng et al[75] reported the synthesis of Ni_3S_2 nanofilms via a hydrothermal method using NF as the precursor reactant and substrate. The obtained material presented a porous carpet-like morphology (see Fig. 3A) of uniform nanostructured Ni_3S_2 films on the NF support and was used as a cathode for LIBs with varying film thickness. As shown in Fig. 3B, an electrode with a 670 nm thick film displayed initial charge and discharge capacities (Q_c and Q_d) of 466 and 596 mAh g^{-1}, respectively, as well as a high reversible capacity of 421 mAh g^{-1} that was obtained after 60 cycles at 50 mA g^{-1}. The thin film electrode also showed over 64% retention of the initial capacity at 5.0 mA cm^{-2}. The authors credited the results to the unique morphology of the thin film and the essential close contact between the film and the NF current collector.

Yang et al[76] applied anodization and thermal annealing techniques to synthesise blooming flower-like NiO nanorods arrays on NF support for application as the binder- and additives-free anodic active material in LIBs. The electrode exhibited discharge and charge capacities of 705.5 and 548.1 mAh g^{-1} after 70 cycles, respectively, with a high coulombic efficiency at 1.0 and 2.0 A g^{-1}. In addition, the electrode showed excellent rate capability as it was able to restore its initial capacity of 945 mAh g^{-1} at 0.5 A g^{-1}.

Zhao et al[77] prepared sulphur nanodots of an average diameter size of 2.0 nm anchored on NF via an electrodeposition route for use as cathode material for lithium-sulphur batteries (LSBs). The synthesis method was undertaken at room temperature with a varied sulphur mass in the range of 0.21 - 4.79 mg cm^{-2}. An electrode with a S content optimized at 0.45 mg cm^{-2} on NF showed an initial Q_d of 1 458 mAh g^{-1} at 0.1C, a high rate capability of 521 mAh g^{-1} at 10C, and excellent cycling stability that gave capacities of 895 mAh g^{-1} (0.5C) and 528 mAh g^{-1} (5.0C) after 300 and1 400 cycles, repectively.

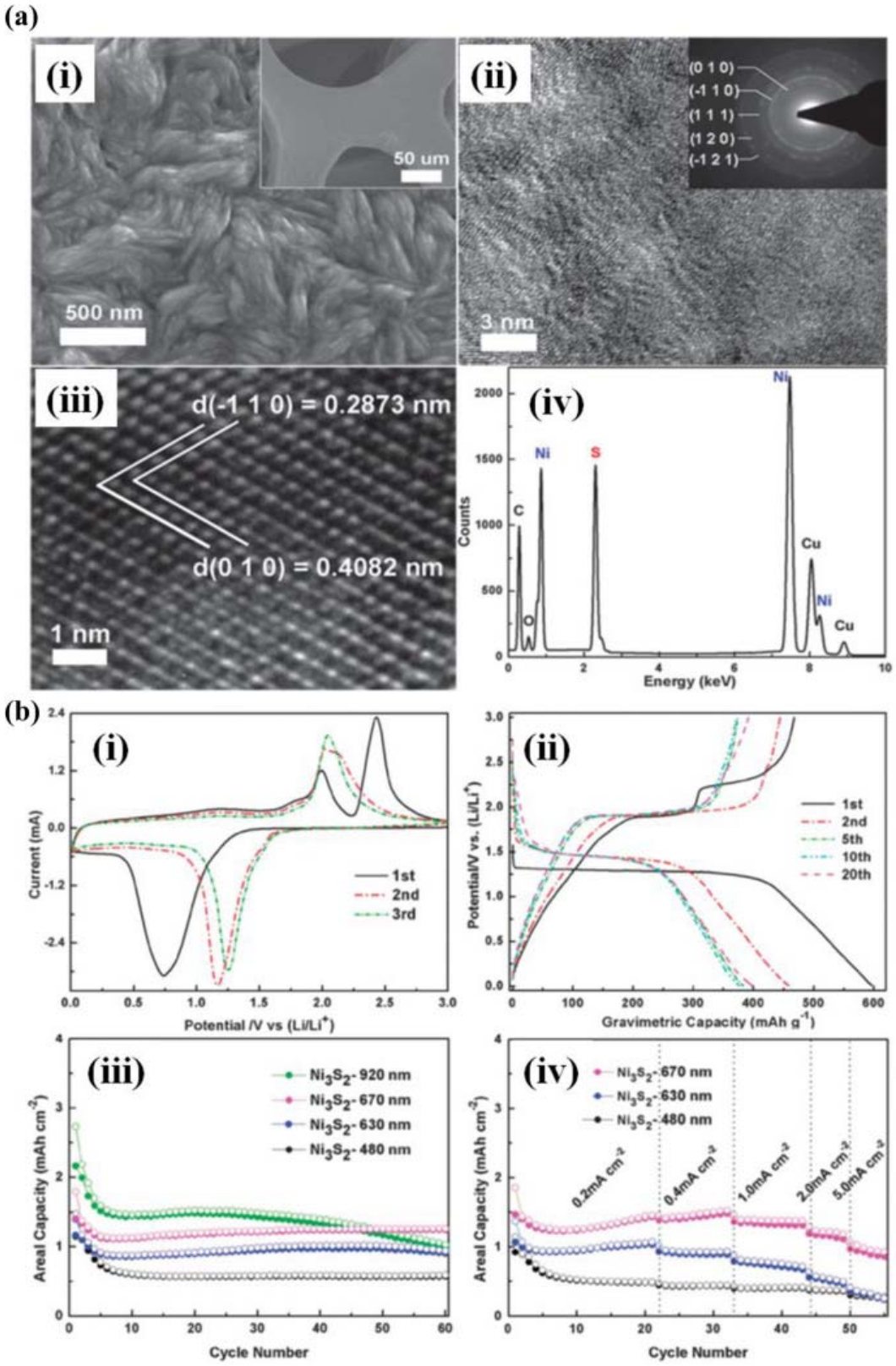

Figure 3: ***(A)*** *morphology and chemical characterization of Ni_3S_2 film, and* ***(B)*** *comparative* ***e****lectrochemical performances of the nanostructured Ni_3S_2 film electrodes. Reprinted (adapted) with permission from Ref.* [75]*. Copyright 2013, Royal Society of Chemistry.*

Zhang et al[78] employed nickel foam foil (NFF) as an interlayer in a LSBs by placing it between the sulphur electrode and the separator in order to suppress the loss of active material and self-discharge of the Li–S system. The group made a comparison of the cell with the rolled NFF to a cell without the NFF, where the former was observed to display enhanced performance with regards to the utilisation of capacity, reversibility, and rate capability. The cell employing the NFF interlayer showed an initial discharge capacity 819 mAh g_S^{-1}, and further showed a discharge capacity of 604 mAh g_S^{-1} (i.e., 74% retention of capacity) after 80 cycles at 0.2C. The counterpart cell (without NFF) achieved an initial capacity of 827 mAh g_S^{-1}, with only 39% capacity retention (324 mAh g_S^{-1}) after 80 cycles at 0.2C. The authors ascribed the improvement in electrochemical performance to the 3D architecture of the NFF interlayer, which was believed to have offered a stable and porous good conductive network that enabled easy migration of the polysulfide to inhibit the charge transfer phenomena that occur during the charge-discharge processes.

Wang et al[79] developed an anode for lithium-oxygen (Li-O_2) batteries by using Bi nanoflakes on NF as active material. The preparation method involved immersing NF in a Bi^{3+}/ethylene glycol solution, where the Bi^{3+}concentration and reaction time-temperature determined the microstructures and thickness of Bi nanoflakes. The Bi/Ni electrode delivered reversible capacities ranging between 377.1 and 206.4 mAh g^{-1}, at a current density range of of 20.0 - 2 000 mA g^{-1}. Furthermore, it reached a high capacity of 302.4 mAh g^{-1} after 100 charge/discharge cycles at 200 mA g^{-1}, as well as a Coulombic efficiency of about 100%, which corresponded to 89% capacity retention.

Hu et al[80] prepared self-supported Ni_3S_2 ultrathin nanosheets via an in-situ hydrothermal method involving the direct sulfurization of NF with thioacetamide as a sulfur source for application as a cathode in alkaline Ni-Zn Battery. The as-prepared Ni_3S_2/Ni electrode exhibited a high capacity of 125 mAh g^{-1} after 100 cycles with no apparent attenuation, an excellent rate capability of 68.0 mAh g^{-1} at 5.0 A g^{-1}. Chen et al[81] employed NF supported NiO nanosheets as cathode active material for Ni-Zn batteries, which showed a volumetric capacity of 3 200 μAh cm^{-3} at 8.0 mA cm^{-2}, as well as a capacity of 979 μAh cm^{-3} at 20.0 mA cm^{-2}. The elecrode also showed energy and power densities of 25.6 mWh cm^{-2} and 86.48 mW cm^{-2}, respectively, as well as good cycling durability of 84.7% capacity retention after 10 000 cycles.

Table 3: *Summary of 3D NF-based electrode materials and their electrochemical performances in battery applications.*

Electrode	Battery	Initial charge/discharge capacity (mAh g^{-1})	Discharge capacity after cycling (mAh g^{-1}) [Cycles]	E_{sp} (mWh cm^{-2})[b]	P_{max} (mW cm^{-2})[c]	Ref.
NiO	LIB	(1.36/ 1.94 mAh cm^{-2})[a]	(1.38 mAh cm^{-2})[a] [140]	-	-	83
Co_3O_4/CuO	LIB	1 310/ 1 633	810 [500]	-	-	84
Co_3O_4 nanowalls	LIB	794/ 1126	835 [100]	-	-	85
Si/rGO	LIB	3 717/ 2 735	2 292 [50]	-	-	86
Sn nanorods	LIB	838.5/ 890	454 [50]	-	-	87
Si@rGO	LIB	1 762/ 2 445	792 [100]	-	-	88
Si-GF	LIB	225/ 326	175 [500]	-	-	89
Co_3O_4-C-NA	ZAB	-	-	-	118	90
MnO_2	ZAB	-	-		95.7	91
Ru nanosheets	Li-CO_2 battery	9 064/ 9 502	Limited to 1 000 [100]	-	-	92
$Na_2Ti_3O_7$	NIB	130/ 300	81.7 [500]	-	-	93
NiSe nanorod	Ni//Zn battery	(1.35/ 1.32 mAh cm^{-2})[a]	(0.74 mAh cm^{-2}) [1 300]	2.26	95.93	94
Co_3O_4-C	ZAB	-	-	-	54.5	95
Fe–NiCoP@C	NAB	-/ (15 Ah L^{-1})[d]	-	-	(621 mW g^{-1})[e]	96
TiO_2 nanoparticles	LAB	1 850/2 000	Limited to 500 [300]	-	-	97

[a] Specific areal capacity (mAh cm^{-2}), [b] Areal energy density, [c] Areal power density, [d] Specific volumetric capacity (Ah L^{-1}, Ah cm^{-3}), [e] Gravimetric power density (mW g^{-1})

In an attempt to develop electrodes with high catalytic activity and stability for oxygen reduction reactions (ORR) in Zn-Air Batteries (ZABs), Wang et al[82] fabricated a continuous mesoporous bimetallic platinum-palladium (PtPd) film on macroporous NF (mPtPd-NF) by soaking NF in a Pt^{2+}/Pd^{3+}/HCl/F127 precursor solution. The mPtPd-NF electrode showed high catalytic performance for ORR that favoured its use as a ZAB electrode. The cell performance

of the electrode was tested against a commercial Pt/C-based ZAB, where it showed a higher open-circuit voltage (OCV) of 1.52 V and a current density of 108 mA cm^{-2} at 1.0 V, compared to the OCV of 0.618 V and current density of 108 mA cm^{-2} of the commercial ZAB. Furthermore, the synthesized electrode showed a power density of 111 mW cm^{-2} at 121.6 mA cm^{-2} compared to 67 mW cm^{-2} of the commercial ZAB, as well as a greater specific capacity and energy density of 613 mAh g_{Zn}^{-1} and 728 Wh kg_{Zn}^{-1} at 10 mA cm^{-2}, respectively, which were higher than those of commercial battery that reached 484 mAh g_{Zn}^{-1} and 541 Wh kg_{Zn}^{-1}, repectively. Table 3 summarises reported literature that involved the use of NF as current collector for battery applications. Table 4 compares the electrochemical performance of NF-based electrodes with that of other current collectors in LIB applications, taking Si nanoparticles as common active material.

Table 4: *Comparative electrochemical performance of Si nanoparticles in LIB applications using NF and other current collectors.*

Current Collector	Specific Capacity (mAh g^{-1})	Capacity Retention (%) [Cycles]	Ref.
Cu foil	2 021	10 [35]	[98]
Cu foam	580	59 [50]	[99]
Carbon nanofiber	1 957	60 [400]	[100]
NF	2 500	80 [100]	[101]
Cu foam	2 745	-	[102]
Cu foil	2 222	-	[103]
Cu foil	3 412	-	[104]
Cu foil	2 143	-	[105]
NF	2 486	57% [50]	[106]
Cu foil	2 375	-	[107]
Cu foil	2 350	-	[107]
Porous Cu	2 550	-	[107]

3.1.3. Fuel Cells

The shift from heavy global reliance on fossil fuels for energy has motivated the race explore and develop clean energy storage and conversion systems like metal-air batteries, fuel cells, and water splitting systems.[108] Fuel cells (FCs) have been highlighted to play a key role in the future energy system, with application in sectors that include large power plants, transportation, and portable devices as they have shown potential to efficiently and reliably convert chemical energy into electric energy; and depending on the fuel type, fuel cells offer a broad and robust operation temperature range and performance at extraordinarily diverse conditions.[109,110] Research emphasis is given to finding alternative fuels and dedicated electrode material.

Rajeshkhanna and Rao[111] synthesized spinel Co_3O_4 nanomaterial with different morphologies directly grown on NF via a simple hydrothermal method and a subsequent calcination process. The NF-supported Co_3O_4 electrodes displayed low onset potential values of 0.34 V for the microflowers, and 0.32 V for both microspheres and nanograss. They also attained current densities of 28, 36.2, and 34.9 A g^{-1} at 0.6 V for the microflowers, microspheres, and nanograss electrodes, respectively. Chronoamperometric tests were done to ascertain the stability and electrocatalytic activity of the electrodes, which followed an increasing chronoamperometric current density trend in the line microflower-Co_3O_4 < nanograss-Co_3O_4 < microsphere-Co_3O_4. A similar order was observed for the cyclic stability tests, which exhibited 32, 66, and 96% retention of the current density after cycling 1 000 times at 10 mV s^{-1}. The authors attributed the better results of the nanograss- and microsphere-Co_3O_4 electrodes to their high surface area and porosity that resulted in the maximum exposure electroactive centres for methanol oxidation.

Wen et al[112] synthesized NF-supported Ni phosphide nanowire arrays (Ni_xP) via a one-step synthetic strategy using hypophosphite as a source of phosphorus (P) and applied the as-synthesized material as a high-performance electrocatalyst for the electro-oxidation of hydrazine in a direct hydrazine fuel cell (DHFC). The group proclaimed the presence of $Ni_{12}P_5$ and Ni_2P phases, which were obtained from the direct phosphorization of commercial NF, with the "Ni_2P nanoparticles entirely distributed on $Ni_{12}P_5$. The Ni_xP/NF electrocatalyst displayed an onset potential (OP) of -0.08 V and a current density of 580 mA cm^{-2} at 0.30 V. It further displayed 80.5% activity retention after 10 000 s of constant-potential measurement and a 14% loss of the electrocatalytic activity after 1 000 CV cycles. The electrode material's excellent electrocatalytic activity was ascribed to the high intrinsic activity, maximum exposure of active

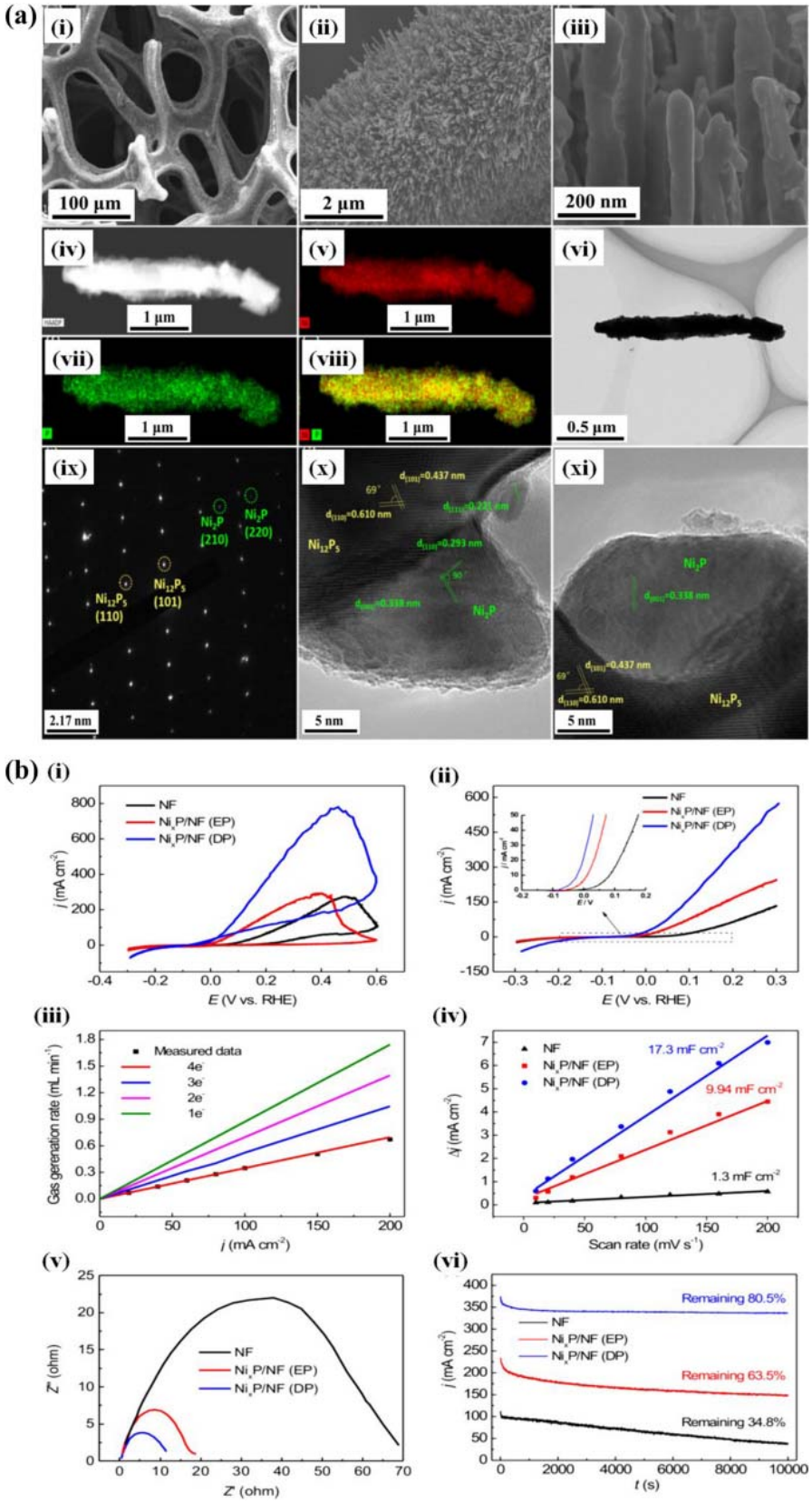

Figure 4: ***(A)*** *morphology and chemical characterization, and* ***(B)*** *comparative* ***e****lectrocatalytic performances Ni_xP/NF (DP) catalyst. Reprinted (adapted) with permission from Ref.* [112]*. Copyright 2019, Elsevier.*

sites on Ni_2P, and the excellent electrical conductivity of both the $Ni_{12}P_5$ and Ni_2P phases. The structural and electrochemical results are demonstrated in Fig. 4.

Ye's group[113] developed a 3D $Ni(OH)_2$/NF electrode for application in direct urea–hydrogen peroxide fuel cells (DUPFCs). The electrode fabricated from $Ni(OH)_2$ nanosheets showed greater urea oxidation compared to the flower-like, sheet-like, and twine-like $Ni(OH)_2$ electrode materials. The nanosheets achieved an oxidation current density of 337 mA cm^{-2} at 0.45 V, as well as an OP of 0.21 V in 0.6 M urea and 5.0 M KOH solutions. Furthermore, as a DUPFC anode, the $Ni(OH)_2$ nanosheet/NF electrode showed an OCV of 0.86 V and maximum power densities of 19.7 mW cm^{-2} and 28.8 mW cm^{-2} at 20 and 50 °C, respectively. Later on, the same group led by Wang, G.[114] synthesised a Ni_2P/NF anode for direct urea fuel cell (DUFC) via a combination of hydrothermal growth and phosphating processes. The obtained Ni_2P@NF electrode displayed porous flower-like nanosheets of Ni_2P on the NF substrate. It showed a low onset oxidation potential of 0.24 V and outstanding stability in 0.6 M urea and 5 M KOH solutions at a scan rate of 15 mV s^{-1}, as well as a current density of 750 mA cm^{-2} at 0.60 V. Table 5 summarises reported literature that involved the use of NF as current collector for FC applications. Table 6 compares the electrochemical performance of NF-based electrodes with that of other current collectors in DMFC applications, taking $NiCo_2O_4$ nanoparticles as common active material.

Table 5: *Summary of 3D NF-based electrode materials and their electrochemical performances in FC applications.*

Electrocatalyst	Fuel Cell	Cell potential [CP) / Onset potential [OP] / Open circuit voltage [OCV] (V)	Current density (mA cm^{-2})	Power density (mW cm^{-2})	Ref.
Co_3O_4 Nanowire	Al–H_2O_2 semi-fuel cell	0.7 (CP)	122	85	[115]
NF	DGFC	0.6 (OCV)	5.03	0.62	[116]
AC	MFC	-0.2 (CP)	0.57	1 190 ± 50	[117]
Pd/graphene aerogel	DMFC/DEFC	-	(798.8/874 A g^{-1})[a]	-	[118]
Pd-Pt/GA	DGFC	0.2 (CP)	6.3	1.25	[119]
Pd-Pt/GA	DEFC	1.0 (CP)	12	3.6	[120]
Pt/NiO-GO	DMFC	0.91(CP)	121.46	-	[121]
Co_3O_4/$NiCo_2O_4$	DMFC	0.6 (CP)	140	-	[122]
Pd_xAu_yGN	DMFC/DEFC	-0.58/-0.74 (OP)	720/1 180	-	[123]
Ni-Mo-S	DGFC	0.16 (CP)	193.2	-	[124]
TiO_2	DUFC	-	0.025	-	[4]
Ni/NiO nanorods	DMFC/DEFC	0.37/0.34 (OP)	479/543	-	[125]
Pd-C/NF	DEFC	0.1 (CP)	400	56.3	[126]
Ni−Co alloy	DHFC	-0.16 (OP)	1 213	-	[127]
NF	PEMFC	0.15 (CP)	6 700	1 890	[128]
NiO/NF/Ag	MCFC	0.87 (OCV)	640	249	[129]
Pd_6Pt@GP	DEFC	0.81 (OP)	141.2	-	[130]
NiO nanosheet	DMFC	1.84 (CP)	300	-	[131]
Co_3O_4	DMFC	1.5 (CP)	233.9	-	[132]
PdAuAg/CNT	DFLFC	0.98 (OCV)	64	16	[133]

[a] Gravimetric current density (A g^{-1})

Table 6: *Comparative electrochemical performance of NiO nanoparticles in DMFC applications using NF and other current collectors.*

Current Collector	Onset potential (V)	Current density ($mA\ cm^{-2}$)	Ref.
NF	0.33	300	[131]
GCE[a]	-	12.54	[134]
Ni foil	-	65	[135]
GCE	0.39	25	[136]
GCE	0.37	6	[136]
NF	-	89	[137]
NF	0.48	222	[138]
GCE	0.70	85.5	[139]
GCE	1.33	24.3	[140]
Au	1.7	12	[141]
Au	1.7	41	[141]

[a] GCE - Glassy Carbon Electrode

3.1.4. Electrochemical Water Splitting

Electrochemical water splitting (EWS) offers the promise of clean and sustainable energy storage and transport through mass hydrogen production.[142] As an alternative fuel, molecular hydrogen has attracted attention in the energy research field because of its great energy density, great energy conversion efficiency, environmental friendliness, and sustainability.[143,144] Therefore, the development of cost-effective and efficient electrocatalysts for the electrochemical generation of H_2 fuel is vital to meeting the world's rising demand for energy, and curbing the progress of global warming.[145] Electrochemical water splitting has been recognised as a commercial technology capable of producing clean hydrogen efficiently and sustainably without the emission of carbonaceous gases.[146–148]

The working principle of EWS is generally characterised by two significant reactions, namely the hydrogen evolution reaction (HER) at the cathode and the oxygen evolution

reaction (OER) at the anode.[149] The efficacy of hydrogen production via electrochemical water splitting is largely affected by the reaction kinetics of the above-mentioned reactions. Large-scale production of high purity hydrogen is flawed by the large overpotential required in an electrolyser due to the sluggish OER.[150] Usually, potentials reaching about 1.8 – 2.0 V, which surpass the theoretical potential (1.23 V) of water degredation, are required to meet the overpotential.

Conversely, the overpotential is determined by the activity of the electrocatalyst during the reaction, i.e., the structural and electronic properties of the catalyst.[151] In practice, good catalysts are required in water electrolysers to enable both operations. The most effective HER catalysts are presently Pt-group metals, while Ir/Ru-based compounds are the standard catalysts for OER. On the other hand, the high cost and scarcity of these precious metals limit their widespread use. A great amount of time and effort have been devoted to the development of non-precious and highly effective electrocatalysts for water electrolysis. Non-precious electrocatalysts include metal sulphides, phosphides, and carbides for HER, as well as metal oxides, phosphates, and hydroxides for OER.[152–154] Most of these electrocatalysts, unlike noble metal-based catalysts, present inferior stability and require greater overpotentials.[155]

Ren and Yuan[12] developed bifunctional non-precious Ni_3S_4 electrocatalyst for electrochemical water splitting. Nanosheets of Ni_3S_4 were directly grown on NF (NiS/NF) by treatment of metallic NF using a one-pot hydrothermal-sulfurization method. The as-prepared NiS/NF electrocatalyst showed good electrocatalytic activity and stability for water electrolysis in alkaline electrolytes. The electrocatalyst only required an OP as low as -122 mV to give a current density of 10.0 mA cm^{-2}, and a Tafel slope that reached a low of 69 mV dec^{-1} during HER evaluation. It also required an OP of 320 mV during OER evaluation to give a current density of 20 mA cm^{-2}, whilst the value of the Tafel slope reached 71 mV dec^{-1}. The authors ascribed the results to the high activity and robust stability of the electrocatalyst that were realised through the integration of the active catalyst onto the conductive metallic NF. The structural and electrochemical studies of the work are shown in Fig. 5.

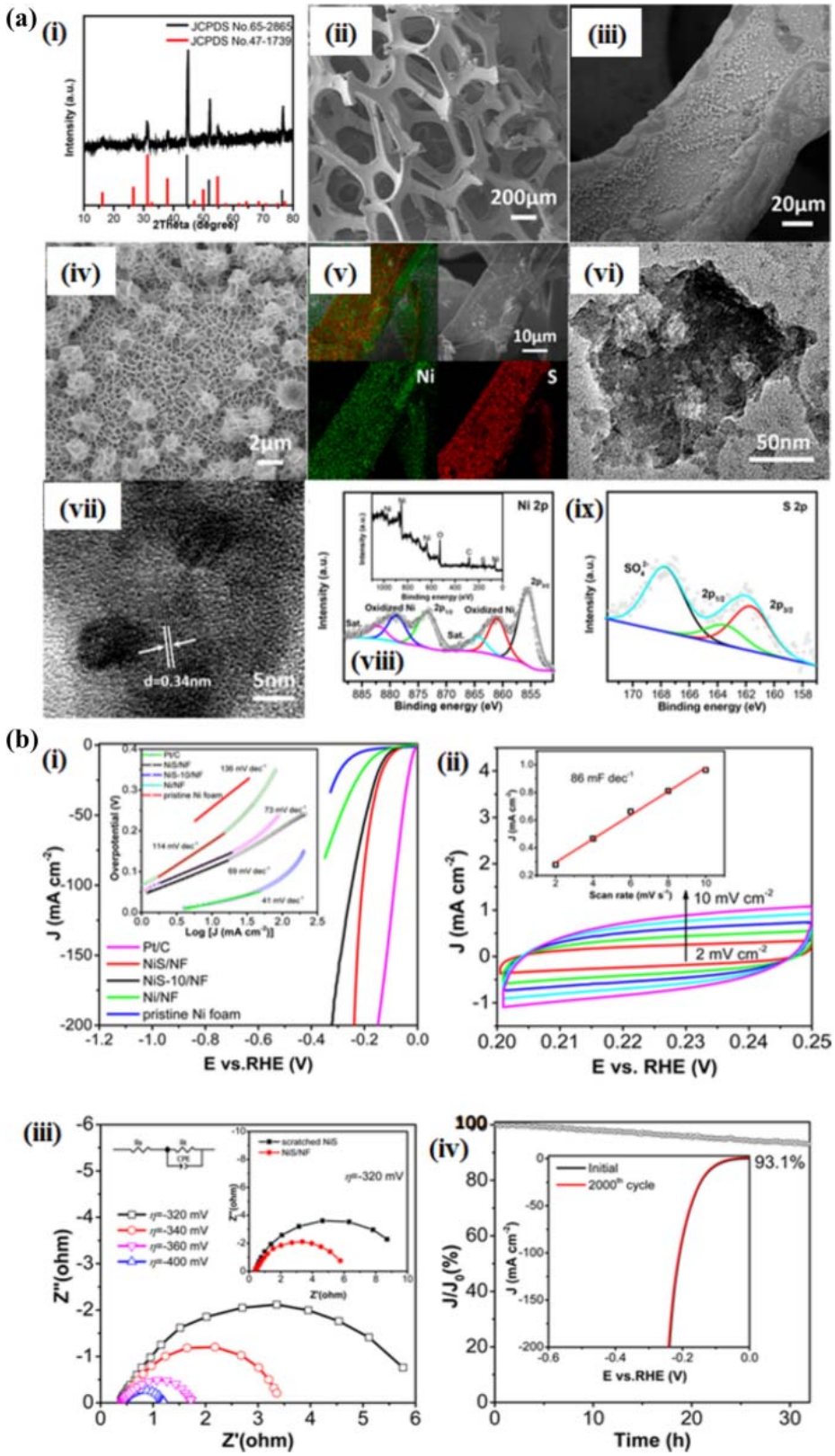

Figure 5: *(**A**) Structural, morphology and chemical characterization of NiS/NF, and (**B**) comparative electrocatalytic performance of Pt/C, NiS/NF, NiS-10/NF, Ni/NF, and pristine Ni foam. Reprinted (adapted) with permission from Ref.* [12]*. Copyright 2017, American Chemical Society.*

Xiao et al[156] synthesised a ternary self-supported electrocatalyst of Fe/Ni phosphides grown on NF as a bifunctional electrode for water splitting. Their study employed a simple thermo-reaction between NaH_2PO_2 and NiFe hydroxide precursors ($NiFe(OH)_x$) to grow $FeNiP_x$ on NF using a chemical precipitation reaction, followed by an oxidation-etching process. The as-prepared electrocatalyst displayed exceptionally high OER and HER activities, with low OP values of 192 and 106, and 236 and 161 mV at 10.0 and 100 mA cm^{-2}, respectively. The electrodes required electrolyser voltages of only 1.53 V and 1.74 V to attain catalytic stability at 10.0 and 50.0 mA cm^{-2} current densities, respectively. The electrocatalyst further showed great stability for both HER and OER, with little degradation observed after 90 h evaluations at 50 mA cm^{-2}. The results obtained in the study were credited to the accumulated synergy of the bimetallic composite, metallic phosphide, and the unique porous nanosheet structure.

A study by Yang et al[157] studied the HER activity of needle-like CoP/rGO electrocatalyst grown on NF via a two-step method involving an initial hydrothermal route for the introduction of Co on the surface of NF and subsequent heat treatment for the introduction of P. The as-prepared CoP/rGO/NF catalytic material displayed excellent HER activity, exhibiting OP and Tafel slope of 136 mV at 50 mA cm^{-2} and 135 mV dec^{-1}, repesctively. The electrocatalyst was also able to demonstrate electrochemical performance stability of at least 25 h in a basic solution. The findings of the study were credited to the material's morphology and the 3D network structure of NF.

In a bid to improve the kinetics of the reaction electrochemical water splitting, Zhou et al[149] explored a series of iron substituted cobalt-nickel phosphides grown on NF (FeCoNi-P/NFs) as potential electrocatalysts for OER. Their study was carried out through a hydrothermal reaction successively followed by a phosphorisation procedure. The as-prepared electrocatalyst exhibited a current density of 100 mA cm^{-2} at an overpotential 286 mV. The FeCoNi-P/NF electrocatalyst needed a potential of 266 mV to drive a current density of 50 mA cm^{-2} a low Tafel slope of 61.2 mV dec^{-1}. The electrocatalyst exhibited good stability of over 60 h in a basic solution. The findings of the study emphasized the significance of heteroatom-substituted TMP on self-supported electrocatalysts. Table 7 summarises reported literature that involved the use of NF as current collector for EWS applications. Table 8 compares the electrochemical performance of NF-based electrodes with that of other current collectors in EWS applications, taking Ni_3S_2 nanoparticles as common active material.

Table 7: *A summary of 3D-NF-based electrode materials and their electrochemical performance in electrochemical water splitting.*

Electrode	Electrolyte	Reaction	Overpotential (mV)	Tafel-slope (mV dec^{-1})	Ref.
Ni-Fe-P@C	1 M KOH	HER/OER	79/217	92.6/40	[150]
Al−Ni−P	0.5 M H_2SO_4	HER	142	75.3	[158]
Co/CoP	1 M NaOH	HER	130	71	[159]
Ni_3S_2	0.1 M KOH	OER	157	159.3	[160]
Ni-B	1 M NaOH	HER/OER	186/360	93/76	[161]
Ni-Mo-P	1 M KOH	OER	140	87.3	[145]
MoS_2/Ni_3S_2	1 M KOH	HER	76	56	[162]
$FePO_4$	1 M KOH	HER/OER	123/218	104.5/42.72	[163]
NiCoS	1 M KOH	OER	370	145	[164]
Fe-β-Ni $(OH)_2$	1 M KOH	OER	219	57	[165]
α-FeOOH	1 M KOH	OER	207	70	[166]
Ni-Se-Mo film	1 M KOH	HER	101	98.9	[167]
MoS_2/Ni_3S_2	1 M KOH	HER	93	85	[168]
CMS	1 M KOH	HER/OER	217/298	48.2/43.9	[169]
NiFeMoS/NF-P	1 M KOH	HER/OER	100/280	121/65	[170]
$ZnCo_2$	1 M KOH	HER/OER	185/278	110.4/64.3	[171]
(P, W)-MoO_2	1 M KOH	HER/OER	89/308	90/286	[172]
V-CoP	1 M KOH	HER/OER	84.6/ 265.3	79.2/66.2	[173]
$NiSe_2@Ni_xS_y$	1 M KOH	HER/OER	148/206	7.48/144.94	[174]
NiFeP-MoO_2	1 M KOH	HER/OER	152/174	80.5/29.4	[175]

Table 8: *Comparative electrochemical performance of Ni_3S_2 nanoparticles in EWS applications using NF and other current collectors.*

Current Collector	Electrolyte	Reaction	Overpotential (mV)	Tafel-slope (mV dec^{-1})	Ref.
NF	0.1 M KOH	OER	157	159.3	[160]
Nickel foil	1 M KOH	HER/OER	135/175	75.7/101.2	[176]
Cu film	0.5 M H_2SO_4	HER	91.6	63.5	[177]
Cu film	1 M KOH	HER	60.8	67.5	[177]
Ag	1 M KOH	HER	-	101	[178]
NF	1 M KOH	HER/OER	116/353	105/51	[179]
Au	1 M KOH	HER/OER	300/400	100/51	[180]
NF	1 M KOH	HER	199.2	106.1	[181]
NF	1 M KOH	OER	223	60.5	[182]
Cu foam	1 M KOH	HER/OER	100/50	98/80	[183]

3.2. Sensors

In recent times, glucose detection has found significant attention due to its application in various fields such as biotechnology clinical diagnostics, food analysis, and fermentation industries.[184–186] Various techniques, which include calorimetry, conductometry, electrochemical methods, and fluorescent-based optical methods, have been used for the detection of glucose in a reliable routine.[187–190] The electrochemical-based glucose sensor has been identified as a standout due to its reliability, sensitivity, selectivity, simple instrumentation and operation, and the promise of easily constructible and low-cost devices.[191–194] In a bid to overcome the challenges encountered with electrochemical enzymatic glucose sensors, [195–197] great research efforts are given to the development of non-enzymatic sensors based on the electrocatalytic oxidation of glucose by nanomaterials,[198,199] which offer advantages like a fast response, excellent sensitivity and an eco-friendly nature.[200] Moreover, the shying away from the high cost and scarce pure precious metals and their alloys (Pt, Au, Pd, Pt–Pb, Pt–Ru, Pt–Au), which possess excellent catalytic activity towards electro-oxidation of glucose and found

wide use for non-enzymatic glucose detection,[201,202] has led to efforts aimed at developing non-precious and low-cost metal-based electrocatalysts.

Lu et al[203] communicated the first use of 3D NF as an effective electrocatalyst for glucose electrooxidation. The electrochemical sensitivity of the electrode was investigated using linear sweeping voltammetry (LSV), which showed an increase in amperometric response as the concentration of glucose in solution was increased. The sensor showed fast amperometric response behaviour by reaching a steady-state current of 94% in 5.0 s. It also exhibited a linear range of 0.05 - 7.35 mM with the correlation coefficient (R) calculated at 0.995, a detection limit (LOD) of 2.2 μM at a S/N ratio (i.e. signal-to-noise ratio) of 3, and superb selectivity for the detection of glucose in the presence of various interfering compounds. A practical application of the sensor was evaluated through the determination of glucose in human blood serum samples. The LSV experiments done on blood serum samples diluted in 0.10 M NaOH showed an increase in the glucose oxidation peak with consecutive addition of glucose into the electrolyte. A linear range of 0.2 to 6 mM was attained with R = 0.997. The NF sensor's repeatability and stability tests of the sensor were determined through storing it in air under ambient conditions and after ten days of storage, the sensor was able to achieve a 96% retention of its initial current response to glucose. Repeated evaluation of the sensor's current response to glucose oxidation after long-term storing gave a relative standard deviation (RSD) of 3.5%, indicating the realible reproducibility of the NF-based sensor. The characterisation results are presented in Fig. 6.

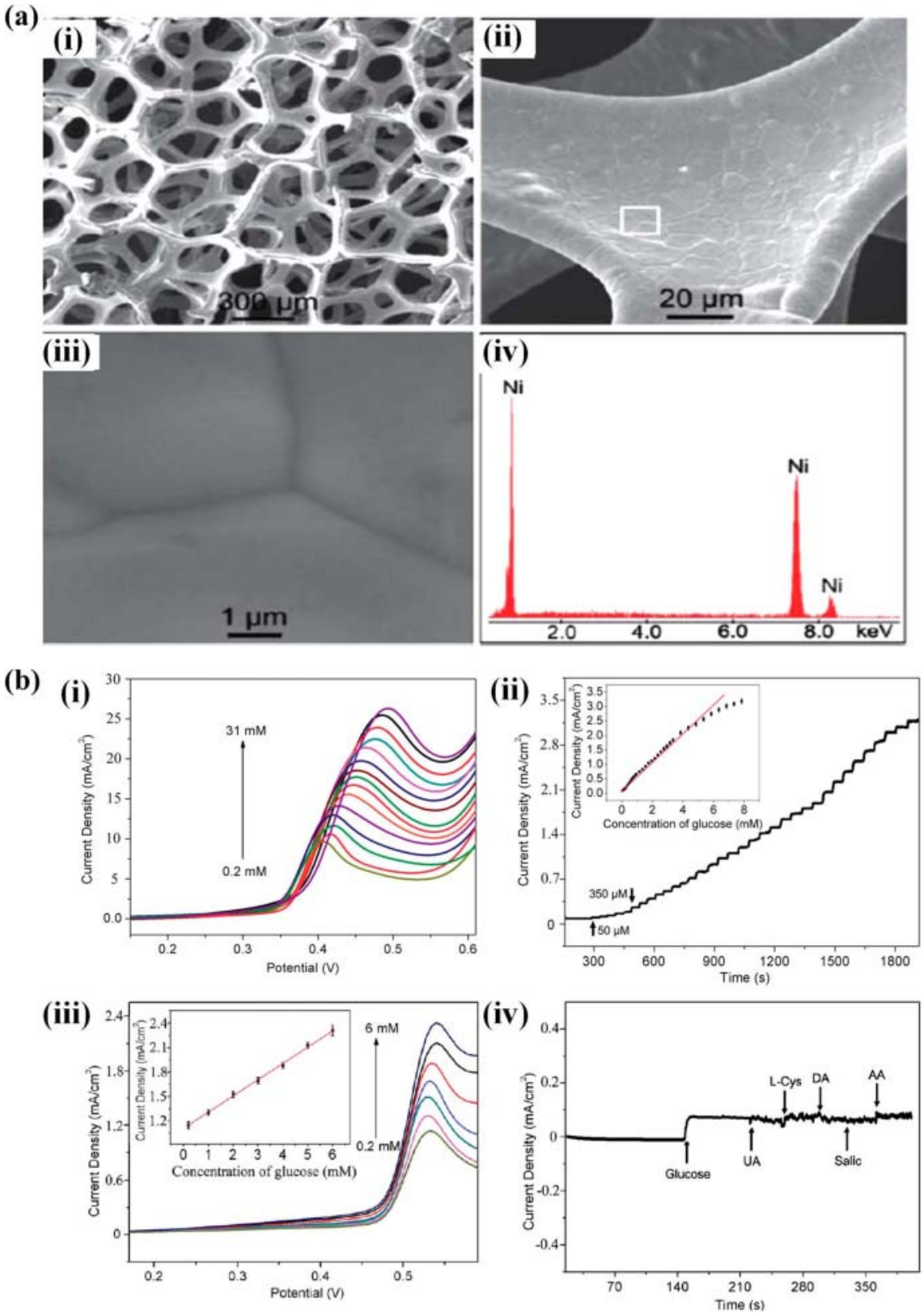

Figure 6: (A) *Morphology and chemical characterization of NF, and* ***(B)*** *comparative electrochemical performance of NF for the detection of glucose. Reprinted (adapted) with permission from Ref.* [203]*. Copyright 2013, The Royal Society of Chemistry.*

Table 9: *NF-based electrocatalysts for the electro-oxidation of glucose in non-enzymatic glucose sensors.*

Electrode	Sensitivity ($\mu A\ mM^{-1}\ cm^{-2}$)	LOD (µM)	Linear range (mM)	Response time (s)	Ref.
NiO	6 657.5	0.46	0.005 - 5.5	< 2	[205]
$Ni(OH)_2$ NPs	1 950.3	0.16	0.6 - 6.0	-	[206]
Ni_3S_2	6 148	1.2	0.005 - 3.0	< 2	[207]
$Ni(OH)_2$ NSs	1 130/1 097	1.0	0.002 - 0.004/0.1 - 2.5	< 2	[208]
NiO	395	6.15	0.018 - 1.2	-	[209]
G-NiO	3 230	< 10	0.01 - 0.2	< 2	[210]
Ni@C	32 794.4	0.05	1.5×10^{-4} - 1.48	-	[211]
NiFe LDH/NF	3 680.2	0.59	0.002 - 0.8	< 1	[212]
$Ni(OH)_2$	2 617.4	2.5	0.0025 - 1.05	-	[213]
Ni-Co-S/PPy core-shell	-	0.82	0.002 - 0.140/0.14 - 2	-	[214]
$NiCo_2O_4$	5 916	0.94	0.001 – 3.987	-	[215]
NiO	499×10^{-3}	1.0	-	< 5	[216]
$ZnCo_2O_4$	16 606	0.15	0.001 - 0.354	-	[217]
$CoTe_2$ nanosheets	168 000	0.59	0.01 - 0.250	0.1	[218]
CuFe-O/GR	0.368	0.0079	7.9×10^{-6} -0.0215	-	[219]
Ni_2P	6 375.1	0.14	0 - 3.0	1	[220]

Chandrasekaran and Matheswaran developed a non-enzymatic glucose sensor using NF coated with a hollow Ni-Al-Mn triple-layered hydroxide (HLTH) nanocomposite.[204] The HLTH/NF electrode reached stability within 3 s and showed an outstanding sensitivity towards glucose oxidation with a wide range of detection from 0.015 - 8 mM. It also exhibited great sensitivity of 2.25 mA mM^{-1} cm^{-2}, with LOD and limit of quantification (LOQ) values calculated at 1.49 µM and 4.51 µM, respectively, at a S/N = 3. Stability studies showed that the electrode was able to retain 97.71% of the current response after 30 days; furthermore, reproducibility and repeatability studies showed RSD values of 3.08 and 2.44%, respectively.

Human blood serum was then used as a real-time sample to investigate the practical application of the electrode. A comparison for the detection of glucose from two different samples with a commercial glucose monitor showed percentage error values of 1.44 and 0.904% for samples 1 and 2, respectively, for the HLTH/NF electrode. Table 9 lists some of the literature reported on NF-based electrodes for non-enzymatic glucose sensors. Table 10 compares the electrochemical performance of NF-based electrodes with that of other current collectors in glucose sensor applications, taking NiO nanoparticles as common active material.

In addition to investigating the capacitive performance of NF-supported porous layered molybdenum selenide-graphene composite ($MoSe_2$-G), Huang, Zhang, and Cai developed a dopamine sensor using the electrode as an electrocatalyst for the oxidation of dopamine.[43] The $MoSe_2$-G/NF electrode showed good electrocatalytic activity for dopamine oxidation within a concentration range of 0.01-10 μM (R = 0.9963), which gave a LOD 1.0 nM (S/N = 3). Furthermore, RSD values of 1.6 and 3.8 % were realised from repeatability and reproducibility studies of the electrode, respectively, as well as long-term stability of 97.5% retention of the initial response after a week. Li, Lu, and Kan[221], prepared a facile electrode through the electrodeposition of gold nanoparticles (AuNPs) and the electro- polymerization of poly(hydroquinone) (pHQ) on the surface NF. The pHQ/AuNPs/NF electrocatalyst was able to exhibit a sensitivity of 6.663 μA μM^{-1} in a linear range of 1.0×10^{-7} - 1.0×10^{-5} M, with a LOD of 4.19×10^{-8} M (S/N = 3). Repeatability studies of the electrode showed an RSD value of 5.7% from the analysis of five different electrodes, whilst stability studies showed a 12.8% attenuation of the reductive peak after storing the electrode for ten days at room temperature. The group further demonstrated the electrocatalyst's excellent selectivity for the dopamine in the presence of hydroquinone, uric acid, glucose, and ascorbic acid, as well as its excellent recovery that varied from 94.0 to 101.0%.

Table 10: *Comparative electrochemical performance of NiO nanoparticles in glucose sensor applications using NF and other current collectors.*

Current Collector	Sensitivity ($\mu A\ mM^{-1}\ cm^{-2}$)	LOD (μM)	Linear range (mM)	Ref.
NF	6 657.5	0.46	0.005 - 5.5	[205]
GCE[a]	1 052.8	1.2	1×10^{-4} – 0.005	[222]
GCE	1 323	0.32	3.2×10^{-5} - 1.1	[223]
Cu foil	4 490	10	0.01 - 8.3	[224]
NF	395	6.15	0.018 - 1.2	[209]
ITO[b]	1 680	0.34	0 - 1	[225]
SPE[c]	1 618.4	2.5	0.25 - 3.75	[226]
Ni foil	4 400	7×10^{-3}	0.5×10^{-3} - 9	[227]
GCE	53.9	0.40	0 - 6	[228]
GCE	400.29	1.0	0 – 0.5	[229]
NF	499×10^{-3}	1.0	-	[216]

[a] GCE – Glassy carbon electrode; [b] ITO - Indium tin oxide; [c] SPE - Screen-printed electrode

Ammonia has found favour as a raw material in various sectors such as agriculture, chemical industry, medical diagnosis, etc. However, environmental dejections like water eutrophication and a threat to aquatic life and the quality of drinking water arise from the pollution of ammonia. This beckons the necessity for the development of aqueous ammonia sensors so as protect water bodies from ammonia pollution. A highlight in this regard was reported by Zhang and company[230] after they fabricated an electrode comprised of platinum nanoparticles-silver/polypyrrole (Pt-Ag/PPy) composite anchored on NF. The electrode displayed good electrocatalytic activity for the oxidation of ammonia, having showed a sensitivity of 0.089 mA μM^{-1} and a LOD estimated at 37 nM (S/N =3). It further showed outstanding selectivity for ammonia amongst various interferents (< 8% interference). Reusability and reproducibility tests conducted on the electrode showed RSD values of 4.7 and

5.4%, while a stability test displayed a 90.3% retention of the original oxidation current after 60 days.

3.3. Waste-Water Treatment

As a consequence of its favourable properties that include high efficiency, versatility, positive impact on the environmental, and low cost, electro-Fenton (EF) has been identified as a stand-out amongst the electrochemical advanced oxidation processes (EAOPs) that have a great potential "green" waste-water treatment.[231–233] The EF process involves a constant in-situ production of H_2O_2 through a series of catalysed reactions as shown in Fig. 7. [234–238] Deng *et al*[234] proposed an unconventional EF system with a NF cathode, and tripolyphosphate (3-PP) as an electrolyte that effectively proved protected the NF cathode against corrosion. Response surface modelling (RSM) estimated the optimum for phenol degradation conditions to be at a pH of 5.8, 3.0 mM of Fe^{2+}, 349.6 mA of current. These conditions ensured a complete degradation in no more than 25.0 min at a rate constant (k_{app}) calculated at 0.2 min^{-1}. The rate constant in this study is over three times (< x3) faster than that of conventional EF/NF systems using a SO_4^{2-} electrolyte of pH = 3. Also, a 81.5% mineralization yield was achived within 2 h. A comprehensive study of the central mechanisms of the oxidation reactions in the EF/NF-3-PP set-up revealed the multifunctional capability of the 3-PP electrolyte, which included the stabilisation of H_2O_2, on top of the Fe^{2+} complexing and the production of additional reactive oxygen. The stabilisation of H_2O_2 by the 3-PP electrolyte resulted in a higher accumulation of the compound as compared to the amount acquired using SO_4^{2-}electrolyte in conventional EF systems. Toxicity studies showed an eventual complete degradation of toxic intermediates that were formed at the early stages of treatment after 2 h.

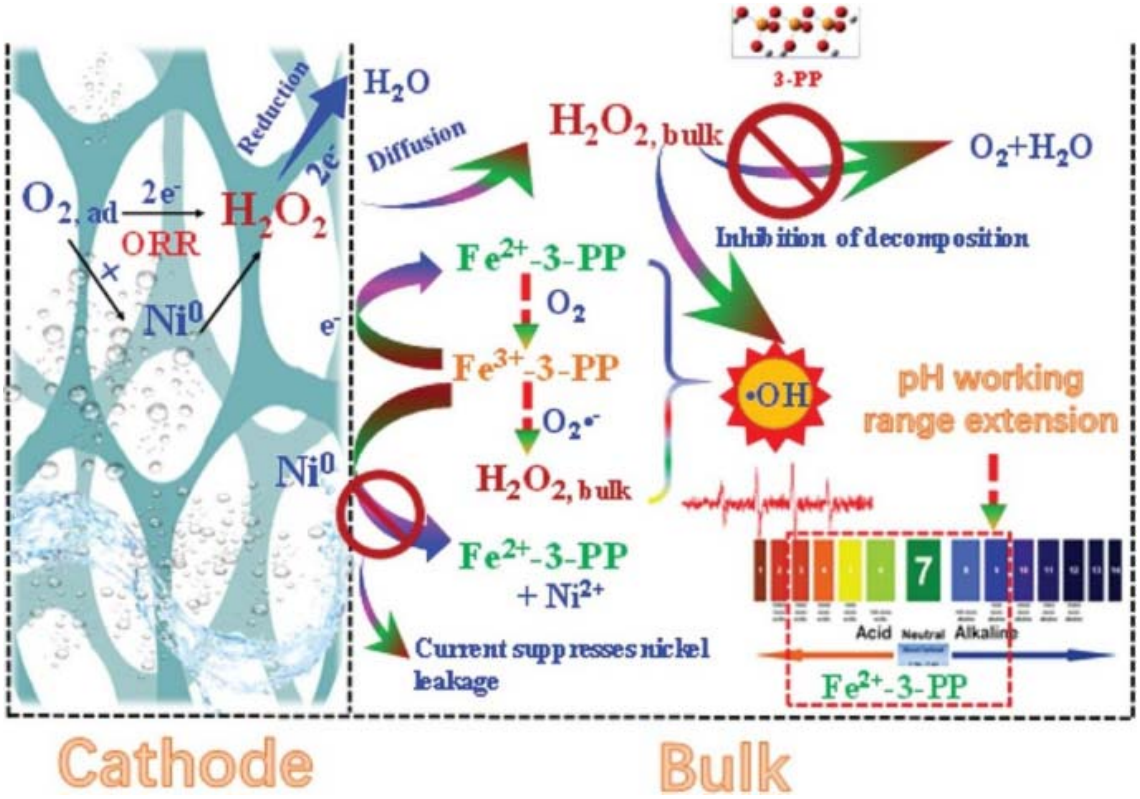

Figure 7: *Graphical representation of the reactions involved in the electro-Fenton (EF) process. Reprinted (adapted) with permission from Ref.* [234]*. Copyright 2020, Elsevier.*

The biodegradation resistant nature of chlorinated aromatic antibiotics and their toxicity because of chlorine atoms pose a threat to aquatic ecosystems and human lives.[239] With reductive dechlorination identified as an effective and realiable waste-water treatment procedure for the removal of the antibiotics,[240–245] numerous techniques have been developed around the concept such as microbial dehalogenation, zero-valent iron reduction, Fenton reactions, and electrocatalytic dechlorination.[246–254] The latter has been receiving great attention due to its high efficiency and generation of less toxic by-products, as well as the circumvention of the need for extra reducing agents.[255–257] Precious metal catalysts have demonstrated the ability to attain high reactivity in the catalytic dechlorination process, with palladium (Pd) exhibiting great retention of the strongly reductive atomic H* in large amounts. This is due to its low OP for HER, as well as its greater H* adsorption and storage capacity.[258–262]

Taking advantage improved reaction kinetics and mild operating conditions of this technology, Yang et al[263] synthesized a Pd@NF electrode through galvanic substitution of Ni atoms on the surface of NF with ultafine Pd nanoparticles. The as-prepared electrode was compared with bare NF and commercial Pd/C the electrochemical dechlorination of the

florfenicol (FLO) antibiotic, where it showed excellent electrocatalytic performance for the intended purpose. The Pd@NF cathode reached a 99.5% dechlorination efficiency of 20 mg L^{-1} FLO, with a fast dechlorination rate of 16.58 mg min^{-1} (at -1.2 V vs. Ag/AgCl). These results surpassed those of the bare NF and commercial Pd/C, which exhibited dechlorination rates of 2.63 mg min^{-1} and 11.32 mg min^{-1}. It also showed a reaction rate constant of 0.044 min^{-1}, which was 44 and 4.4 times faster than the 0.001 min^{-1} and 0.010 min^{-1} observed for the bare NF and commercial Pd/C electrodes, respectively. Furthermore, the electrode showed excellent stability with 95% of the FLO removal efficiency still attained after 20 cycles. The authors attributed the excellent electrocatalytic performance of the Pd@NF electrode for FLO dechlorination to the enhanced mass transfer due to the presence of the 3D independently supported NF frame and the micro-interfaces of Pd-Ni on the surface of NF that led to improved utilization of H*.

Lou et al[264] prepared a Pd/MnO_2/NF as a hydrodechlorination (ECH) electrocatalyst via an electrodeposition method. The introduction of MnO_2 was found to have immensely improved the catalytic activity of the electrocatalyst and effectively reduced the amount of dose Pd compared to the common Pd/NF electrode. The electrocatalyst required only one-fourth of Pd in compare to Pd/NF, with dechlorination of 2,4-dichlorobenzoic acid (2,4-DCBA) being completely achieved under 2 h. Repeatability studies showed a slight decrease in the 2,4-DCBA removal efficiency, with 100, 98, 98, 95, and 94% removal efficiencies observed in five consecutive tests. Mechanistic examinations showed that the dechlorination process was dominated by the atomic H∗-based indirect pathway, with roughly 13% removal of 2,4-DCBA achieved through direct electron transfer. The MnO_2 nanoparticles were observed to have provided Pd with more atomic H* through the enhancement of the water dissociation and hydrogen evolution reactions.

3.4. Ammonia Synthesis

The electrochemical synthesis of ammonia is considered as an alternative green method to the traditional Haber−Bosch process due to the reduced energy consumption and mild operation conditions,[265–272] as outlined in Table 4. An emphasis is given to the design and development of efficient electrocatalysts for facile adsorption and activation of nitrogen for the nitrogen reduction reaction (NRR). The direct growth of porous metallic nanostructures on conductive substrates like NF has been identified as a solution to the various challenges encountered with

the fabrication and use of porous noble metals as electrocatalysts as it offers timeously fabricated electrodes with more electro-active sites and heightened conductivity.[273,274]

Wang et al[273] used an electrochemical method involving a micelle electrodeposition process to coat a porous Au film onto NF to fabricate an electrocatalyst for the reduction of nitrogen to ammonia. The electrode, denoted as pAu/NF, demonstrated great NRR efficieny, with the NH_3 yield rate (r_{NH_3}) peaking at 9.42 μg h^{-1} cm^{-2}, as well as good Faradaic efficiency (FE) calculated at 13.36% at -0.20 V in 0.1 M Na_2SO_4. The electrode also showed improved selectivity for the reduction of nitrogen to ammonia than to the formation hydrazine (N_2H_2). Chronoamperometric tests (CA) of the pAu/NF displayed an insignificant degradation of the current density after 20 h electrolysis, while a slight reduction in the r_{NH_3} was observed from stability. The NRR results of the pAu/NF electrode were ascribed to the its porous architecture and the optimized composition of active Au.

Table 11: *Comparison between the Haber-Bosch process and the Electrocatalytic nitrogen reduction reaction for the production of NH_3.*

	Haber−Bosch (H−B)	**Electrocatalytic Nitrogen Reduction Reaction (NRR)**
Temperature (°C)	350−550	Ambient (~25 °C)
Pressure (MPa)	15−35	Ambient (~0.1 MPa)
Reagents	N_2, O_2,CH_4 and H_2O	N_2 and H_2O
By-product	CO_2	-

A slightly different group led by Wang, Z.[275] followed suit with the synthesis method to grow a Pd film with tailored pore-sizes on NF. The electrode, designated as nPd/NF, exhibited an excellent catalytic NRR performance for the production of ammonia, with high r_{NH_3} and FE of 18.27 μg h^{-1} mg_{cat}^{-1} and 10.36% in 0.1 M Na_2SO_4, respectively. Furthermore, the electrode showed excellent selectivity for the production of ammonia, as well as excellent long-term durability with high r_{NH_3} and FE values of 17.98 μg h^{-1} mg_{cat}^{-1} and 10.03% were obtained in chronoamperometric test that lasted for 20 h. The catalytic performance of the electrode was

ascribed to the combination of the continuous large nano-porous structure and the self-supported properties.

A similar group led by Yu, H.[274], used the same method to prepare a mesoporous Au_3Pd film-coated NF electrode. The as-fabricated mAu_3Pd/NF electrode showed higher NRR catalytic activity with r_{NH_3} = 24.02 μg h^{-1} mg_{cat}^{-1} and FE = 18.16%. The electrode further demonstrated ideal long-term stability with a slight attenuation of current, evidenced by high r_{NH_3} and FE constants after 20 h. The authors credited the superb NRR performance of mAu_3Pd/NF electrode to the synergistic effect of the Au-Pd bimetallic composition and electronic activity of the self-supported mesoporous film structure.

Li et al[276] also adopted the micelle electrodeposition method to synthesise interweaved porous palladium-ruthenium nanosheets coated on NF (PdRu NS-NF) for the electrocatalytic production of ammonia through nitrogen production. The PdRu NS-NF electrode exhibited maximum r_{NH_3} and FE values of 20.46 mg h^{-1} cm^{-2} (34.1 mg h^{-1} mg_{cat}^{-1}) and 2.11%, respectively. Five recycling tests were undertaken to determine the stability of the electrode, with a retention of 96% of the values r_{NH_3} and FE constants, as well as a slight attenuation of the current density after 30 h electrolysis. In addition, a negligible decrease was observed from the initial r_{NH_3} and FE values after a long-term stability test. The unique structure of the PdRu NS-NF electrode was credited with excellent NRR performance as it provided a large number of electro-active sites and convenient pathways for charge/mass transfer, thus enhancing the electrocatalytic efficiency of the electrode.

4. Conclusion and Future Perspectives

Nickel foam has over the years become very popular with researchers as a current collector of choice in electrochemical systems that include energy storage and conversion, sensors, waste-water treatment, ammonia synthesis, etc. However, some concerns have been raised about the contribution of NF as a current collector to the performance of some electrochemical devices. This contribution was attributed to the existence of electroactive chemical species on the surface of NF. On the other hand, the majority of studies involving NF as a current collector reported negligible contribution of NF to the overall performance. In comparison to other current collectors, NF-supported active materials demonstrated improved electrochemical performance which was mostly attributed to the unique properties of NF. Also, the ability to use NF as a substrate to grow electroactive materials directly on its surface has proven to be an

effective approach to relatively reducing the cost of electrode fabrication for fundamental research. This strategy eliminates the need for additives such as binding and conducting materials, which could translate to a reduced total cost of the device manufacture and improved electrochemical performance due to maximum exposure of the electroactive material. Thus, a scaled-up commercial-level study of the strategy is necessary to validate it as a cost-effective route for electrode development and enhancing device performance. As evidenced in this review, there is a growing interest in the use of NF due to its unique properties that are favorable in various electrochemical systems. However, a comprehensive study of the NF's chemistry in these systems is still required to ascertain its impact on the overall electrochemical performance. Also, a detailed analysis is necessary for the comparison of NF with other current collectors to establish a guideline for the future selection of compatible current collectors for specific electrochemical applications. A case-by-case study of using NF in various electrolytes is necessary to eliminate any discrepancies in the communication of the literature involving NF, such as that observed in some literature reports.

Acknowledgements

MSR would like to thank the financial support from the Gauteng City-Region Academy (GCRA). BLOP would like to thank the financial support from the Learning Academy of the Department of Water and Sanitation. KM and KDM, would like to thank the financial support from the National Research Foundation, South Africa under the Thuthuka programme (UID Nos. 117984, and 118113) and the Competitive Support for Unrated Researchers (UID No. 138085).

Disclosure statements

Conflict of Interest: There are no conflicts of interest declared by the authors.

Funding: The research received no outside funding.

Compliance with Ethical Standards: There are no studies using human or animal subjects in this article.

References

(1) Salleh, N. A.; Kheawhom, S.; Mohamad, A. A. Characterizations of Nickel Mesh and Nickel Foam Current Collectors for Supercapacitor Application. *Arab. J. Chem.* **2020**, *13* (8), 6838–6846. https://doi.org/10.1016/j.arabjc.2020.06.036.

(2) Makgopa, K.; Bello, A.; Raju, K.; Modibane, K. D.; Hato, M. J. Nanostructured Metal Oxides for Supercapacitor Applications. In *Emerging Nanostructured Materials for Energy and Environmental Science*; Rajendran S., Naushad M., Raju K., B. R., Ed.; Springer, 2019; pp 247–303. https://doi.org/10.1007/978-3-030-04474-9_6.

(3) Pant, B.; Ojha, G. P.; Park, M. One-Pot Synthesis, Characterization, and Electrochemical Studies of Tin-Nickel Sulfide Hybrid Structures on Nickel Foam for Supercapacitor Applications. *J. Energy Storage* **2020**, *32* (October), 101954. https://doi.org/10.1016/j.est.2020.101954.

(4) Alami, A. H.; Abdelkareem, M. A.; Faraj, M.; Aokal, K.; Al Safarini, N. Titanium Dioxide-Coated Nickel Foam Photoelectrodes for Direct Urea Fuel Cell Applications. *Energy* **2020**, *208*, 118253. https://doi.org/10.1016/j.energy.2020.118253.

(5) Lefebvre, L. P.; Banhart, J.; Dunand, D. C. Porous Metals and Metallic Foams: Current Status and Recent Developments. *Adv. Eng. Mater.* **2008**, *10* (9), 775–787. https://doi.org/10.1002/adem.200800241.

(6) Nanoshel. Nickel Foam Industrial Application https://www.nanoshel.com/nickel-foam-industrial-application (accessed Aug 4, 2021).

(7) Guan, C.; Liu, J.; Cheng, C.; Li, H.; Li, X.; Zhou, W.; Zhang, H.; Fan, H. J. Hybrid Structure of Cobalt Monoxide Nanowire @ Nickel Hydroxidenitrate Nanoflake Aligned on Nickel Foam for High-Rate Supercapacitor. *Energy Environ. Sci.* **2011**, *4* (11), 4496–4499. https://doi.org/10.1039/c1ee01685g.

(8) Yu, D.; Li, Z.; Zhao, G.; Zhang, H.; Aslan, H.; Li, J.; Sun, F.; Zhu, L.; Du, B.; Yang, B.; Cao, W.; Sun, Y.; Besenbacher, F.; Yu, M. Porous Ultrathin NiSe Nanosheet Networks on Nickel Foam for High-Performance Hybrid Supercapacitors. *ChemSusChem* **2020**, *13* (1), 260–266. https://doi.org/10.1002/cssc.201901766.

(9) Yu, M.; Wang, W.; Li, C.; Zhai, T.; Lu, X.; Tong, Y. Scalable Self-Growth of Ni@NiO Core-Shell Electrode with Ultrahigh Capacitance and Super-Long Cyclic Stability for Supercapacitors. *NPG Asia Mater.* **2014**, *6* (9), e129. https://doi.org/10.1038/am.2014.78.

(10) Makgopa, K.; Ejikeme, P. M.; Jafta, C. J.; Raju, K.; Zeiger, M.; Presser, V.; Ozoemena, K. I. A High-Rate Aqueous Symmetric Pseudocapacitor Based on Highly Graphitized Onion-like Carbon/Birnessite-Type Manganese Oxide Nanohybrids. *J. Mater. Chem. A* **2015**, *3* (7), 3480–3490. https://doi.org/10.1039/c4ta06715k.

(11) Xing, W.; Qiao, S.; Wu, X.; Gao, X.; Zhou, J.; Zhuo, S.; Hartono, S. B.; Hulicova-Jurcakova, D. Exaggerated Capacitance Using Electrochemically Active Nickel Foam as Current Collector in Electrochemical Measurement. *J. Power Sources* **2011**, *196* (8), 4123–4127. https://doi.org/10.1016/j.jpowsour.2010.12.003.

(12) Ren, J. T.; Yuan, Z. Y. Hierarchical Nickel Sulfide Nanosheets Directly Grown on Ni Foam: A Stable and Efficient Electrocatalyst for Water Reduction and Oxidation in Alkaline Medium. *ACS Sustain. Chem. Eng.* **2017**, *5* (8), 7203–7210. https://doi.org/10.1021/acssuschemeng.7b01419.

(13) Yao, K.; Zhai, M.; Ni, Y. α-Ni(OH) 2 ·0.75H 2 O Nanofilms on Ni Foam from Simple NiCl 2 Solution: Fast Electrodeposition, Formation Mechanism and Application as an Efficient Bifunctional Electrocatalyst for Overall Water Splitting in Alkaline Solution. *Electrochim. Acta* **2019**, *301*, 87–96. https://doi.org/10.1016/j.electacta.2019.01.152.

(14) Yang, X. G.; Duan, D. L.; Zhang, X.; Jiang, S. L.; Li, S.; Zhang, H. C. Impact Behavior of Polyetheretherketone/Nickel Foam Co-Continuous Composites. *J. Mater. Eng. Perform.* **2019**, *28* (10), 6380–6390. https://doi.org/10.1007/s11665-019-04360-0.

(15) Geaney, H.; McNulty, D.; O'Connell, J.; Holmes, J. D.; O'Dwyer, C. Assessing Charge Contribution from Thermally Treated Ni Foam as Current Collectors for Li-Ion Batteries. *J. Electrochem. Soc.* **2016**, *163* (8), A1805–A1811. https://doi.org/10.1149/2.0071609jes.

(16) Alami, A. H.; Aokal, K.; Faraj, M. Investigating Nickel Foam as Photoanode Substrate for Potential Dye-Sensitized Solar Cells Applications. *Energy* **2020**, *211*, 118689. https://doi.org/10.1016/j.energy.2020.118689.

(17) Shinde, P. A.; Seo, Y.; Lee, S.; Kim, H.; Pham, Q. N.; Won, Y.; Chan Jun, S. Layered Manganese Metal-Organic Framework with High Specific and Areal Capacitance for Hybrid Supercapacitors. *Chem. Eng. J.* **2020**, *387* (July 2019), 122982. https://doi.org/10.1016/j.cej.2019.122982.

(18) Jiang, Y.; Lu, Y.; Lin, J.; Wang, X.; Shen, Z. A Hierarchical MoP Nanoflake Array Supported on Ni Foam: A Bifunctional Electrocatalyst for Overall Water Splitting. *Small Methods* **2018**, *2* (5), 1700369. https://doi.org/10.1002/smtd.201700369.

(19) Oyedotun, K. O.; Momodu, D. Y.; Naguib, M.; Mirghni, A. A.; Masikhwa, T. M.; Khaleed, A. A.; Kebede, M.; Manyala, N. Electrochemical Performance of Two-Dimensional Ti 3 C 2 -Mn 3 O 4 Nanocomposites and Carbonized Iron Cations for Hybrid Supercapacitor Electrodes. *Electrochim. Acta* **2019**, *301*, 487–499. https://doi.org/10.1016/j.electacta.2019.01.158.

(20) Conway, B. E. *Electrochemical Supercapacitors*; Springer US: Boston, MA, 1999. https://doi.org/10.1007/978-1-4757-3058-6.

(21) Simon, P.; Gogotsi, Y. Materials for Electrochemical Capacitors. In *Nanoscience and Technology: A Collection of Reviews from Nature Journals*; Co-Published with Macmillan Publishers Ltd, UK, 2009; Vol. 7, pp 320–329. https://doi.org/10.1142/9789814287005_0033.

(22) Miller, J. R. Valuing Reversible Energy Storage. *Science (80-.).* **2012**, *335* (6074), 1312–1313. https://doi.org/10.1126/science.1219134.

(23) Frackowiak, E.; Béguin, F. Carbon Materials for the Electrochemical Storage of Energy in Capacitors. *Carbon N. Y.* **2001**, *39* (6), 937–950.

https://doi.org/10.1016/S0008-6223(00)00183-4.

(24) Yuan, K.; Xu, Y.; Uihlein, J.; Brunklaus, G.; Shi, L.; Heiderhoff, R.; Que, M.; Forster, M.; Chassé, T.; Pichler, T.; Riedl, T.; Chen, Y.; Scherf, U. Straightforward Generation of Pillared, Microporous Graphene Frameworks for Use in Supercapacitors. *Adv. Mater.* **2015**, *27* (42), 6714–6721. https://doi.org/10.1002/adma.201503390.

(25) Choudhary, N.; Li, C.; Moore, J.; Nagaiah, N.; Zhai, L.; Jung, Y.; Thomas, J. Asymmetric Supercapacitor Electrodes and Devices. *Adv. Mater.* **2017**, *29* (21). https://doi.org/10.1002/adma.201605336.

(26) Largeot, C.; Portet, C.; Chmiola, J.; Taberna, P. L.; Gogotsi, Y.; Simon, P. Relation between the Ion Size and Pore Size for an Electric Double-Layer Capacitor. *J. Am. Chem. Soc.* **2008**, *130* (9), 2730–2731. https://doi.org/10.1021/ja7106178.

(27) Teffu, D. M.; Makhafola, M. D.; Ndipingwi, M. M.; Makhado, E.; Hato, M. J.; Iwuoha, E. I.; Modibane, K. D.; Makgopa, K. Interrogation of Electrochemical Performance of Reduced Graphene Oxide/Metal-Organic Framework Hybrid for Asymmetric Supercabattery Application. *Electroanalysis* **2020**, *32* (12), 2827–2837. https://doi.org/10.1002/elan.202060303.

(28) Makgopa, K.; Mabena, L. F.; Brink, C. G.; Chauke, G. N.; Teffu, M. D.; Modibane, K. D.; Hato, M. J. Nanostructured Carbon-Based Electrode Materials for Supercapacitor Applications. In *Carbon Related Materials*; Kaneko, S., Aono, M., Pruna, A., Can, M., Mele, P., Ertugrul, M., Endo, T., Eds.; Springer Singapore: Singapore, 2021; pp 317–355. https://doi.org/10.1007/978-981-15-7610-2_14.

(29) Makgopa, K.; Ratsoma, M. S.; Raju, K.; Mabena, L. F.; Modibane, K. D. One-Step Hydrothermal Synthesis of Nitrogen-Doped Reduced Graphene Oxide/Hausmannite Manganese Oxide for Symmetric and Asymmetric Pseudocapacitors. *ACS Omega* **2021**, *6* (47), 31421–31434. https://doi.org/10.1021/acsomega.1c02302.

(30) Zhang, Q.; Xu, C.; Lu, B. Super-Long Life Supercapacitors Based on the Construction of Ni Foam/Graphene/Co3S4 Composite Film Hybrid Electrodes. *Electrochim. Acta* **2014**, *132*, 180–185. https://doi.org/10.1016/j.electacta.2014.03.111.

(31) Jiang, S.; Wu, J.; Ye, B.; Fan, Y.; Ge, J.; Guo, Q.; Huang, M. Growth of Ni3Se2 Nanosheets on Ni Foam for Asymmetric Supercapacitors. *J. Mater. Sci. Mater. Electron.* **2018**, *29* (6), 4649–4657. https://doi.org/10.1007/s10854-017-8416-y.

(32) Zhang, F.; Yuan, C.; Lu, X.; Zhang, L.; Che, Q.; Zhang, X. Facile Growth of Mesoporous Co 3O 4 Nanowire Arrays on Ni Foam for High Performance Electrochemical Capacitors. *J. Power Sources* **2012**, *203*, 250–256. https://doi.org/10.1016/j.jpowsour.2011.12.001.

(33) Yuan, C.; Li, J.; Hou, L.; Zhang, X.; Shen, L.; Lou, X. W. Ultrathin Mesoporous NiCo 2O 4 Nanosheets Supported on Ni Foam as Advanced Electrodes for Supercapacitors. *Adv. Funct. Mater.* **2012**, *22* (21), 4592–4597. https://doi.org/10.1002/adfm.201200994.

(34) Ye, S.; Feng, J.; Wu, P. Deposition of Three-Dimensional Graphene Aerogel on Nickel Foam as a Binder-Free Supercapacitor Electrode. *ACS Appl. Mater. Interfaces* **2013**, *5*

(15), 7122–7129. https://doi.org/10.1021/am401458x.

(35) Yang, J.; Zhang, E.; Li, X.; Yu, Y.; Qu, J.; Yu, Z. Z. Direct Reduction of Graphene Oxide by Ni Foam as a High-Capacitance Supercapacitor Electrode. *ACS Appl. Mater. Interfaces* **2016**, *8* (3), 2297–2305. https://doi.org/10.1021/acsami.5b11337.

(36) Raju, K.; Han, H.; Velusamy, D. B.; Jiang, Q.; Yang, H.; Nkosi, F. P.; Palaniyandy, N.; Makgopa, K.; Bo, Z.; Ozoemena, K. I. Rational Design of 2D Manganese Phosphate Hydrate Nanosheets as Pseudocapacitive Electrodes. *ACS Energy Lett.* **2020**, *5* (1), 23–30. https://doi.org/10.1021/acsenergylett.9b02299.

(37) Mahmoud, B. A.; Mirghni, A. A.; Oyedotun, K. O.; Fasakin, O.; Manyala, N. Nanoplatelets Ammonium Nickel-Cobalt Phosphate Graphene Foam Composite as Novel Electrode Material for Hybrid Supercapacitors. *J. Alloys Compd.* **2021**, *883*, 160897. https://doi.org/10.1016/j.jallcom.2021.160897.

(38) Teffu, D. M.; Ramoroka, M. E.; Makhafola, M. D.; Makgopa, K.; Maponya, T. C.; Seerane, O. A.; Hato, M. J.; Iwuoha, E. I.; Modibane, K. D. High-Performance Supercabattery Based on Reduced Graphene Oxide/Metal Organic Framework Nanocomposite Decorated with Palladium Nanoparticles. *Electrochim. Acta* **2022**, *412*, 140136. https://doi.org/https://doi.org/10.1016/j.electacta.2022.140136.

(39) Yu, L.; Zhang, G.; Yuan, C.; Lou, X. W. Hierarchical NiCo2O4@MnO2 Core-Shell Heterostructured Nanowire Arrays on Ni Foam as High-Performance Supercapacitor Electrodes. *Chem. Commun.* **2013**, *49* (2), 137–139. https://doi.org/10.1039/c2cc37117k.

(40) Guo, D.; Zhang, P.; Zhang, H.; Yu, X.; Zhu, J.; Li, Q.; Wang, T. NiMoO4 Nanowires Supported on Ni Foam as Novel Advanced Electrodes for Supercapacitors. *J. Mater. Chem. A* **2013**, *1* (32), 9024–9027. https://doi.org/10.1039/c3ta11487b.

(41) Wang, B.; Liu, Q.; Qian, Z.; Zhang, X.; Wang, J.; Li, Z.; Yan, H.; Gao, Z.; Zhao, F.; Liu, L. Two Steps in Situ Structure Fabrication of Ni-Al Layered Double Hydroxide on Ni Foam and Its Electrochemical Performance for Supercapacitors. *J. Power Sources* **2014**, *246*, 747–753. https://doi.org/10.1016/j.jpowsour.2013.08.035.

(42) Chen, H.; Jiang, J.; Zhang, L.; Xia, D.; Zhao, Y.; Guo, D.; Qi, T.; Wan, H. In Situ Growth of NiCo2S4 Nanotube Arrays on Ni Foam for Supercapacitors: Maximizing Utilization Efficiency at High Mass Loading to Achieve Ultrahigh Areal Pseudocapacitance. *J. Power Sources* **2014**, *254*, 249–257. https://doi.org/10.1016/j.jpowsour.2013.12.092.

(43) Huang, K. J.; Zhang, J. Z.; Cai, J. L. Preparation of Porous Layered Molybdenum Selenide-Graphene Composites on Ni Foam for High-Performance Supercapacitor and Electrochemical Sensing. *Electrochim. Acta* **2015**, *180*, 770–777. https://doi.org/10.1016/j.electacta.2015.09.016.

(44) Kuang, M.; Liu, X. Y.; Dong, F.; Zhang, Y. X. Tunable Design of Layered CuCo2O4 Nanosheets@MnO2 Nanoflakes Core-Shell Arrays on Ni Foam for High-Performance Supercapacitors. *J. Mater. Chem. A* **2015**, *3* (43), 21528–21536. https://doi.org/10.1039/c5ta05957g.

(45) Xu, X.; Zhao, H.; Zhou, J. K.; Xue, R.; Gao, J. NiCoO2 Flowers Grown on the Aligned-Flakes Coated Ni Foam for Application in Hybrid Energy Storage. *J. Power Sources* **2016**, *329*, 238–246. https://doi.org/10.1016/j.jpowsour.2016.08.080.

(46) Wang, X.; Hao, J.; Su, Y.; Liu, F.; An, J.; Lian, J. A Ni1-: XZnxS/Ni Foam Composite Electrode with Multi-Layers: One-Step Synthesis and High Supercapacitor Performance. *J. Mater. Chem. A* **2016**, *4* (33), 12929–12939. https://doi.org/10.1039/c6ta04022e.

(47) Ozoemena, K. I.; Raju, K.; Ejikeme, P. M.; Ozoemena, K. I. High-Performance Mn3O4/Onion-like Carbon (OLC) Nanohybrid Pseudocapacitor: Unravelling the Intrinsic Properties of OLC against Other Carbon Supports. *Carbon N. Y.* **2017**, *117*, 20–32. https://doi.org/10.1016/j.carbon.2017.02.050.

(48) Lamiel, C.; Nguyen, V. H.; Kumar, D. R.; Shim, J. J. Microwave-Assisted Binder-Free Synthesis of 3D Ni-Co-Mn Oxide Nanoflakes@Ni Foam Electrode for Supercapacitor Applications. *Chem. Eng. J.* **2017**, *316*, 1091–1102. https://doi.org/10.1016/j.cej.2017.02.004.

(49) Kong, S.; Yang, F.; Cheng, K.; Ouyang, T.; Ye, K.; Wang, G.; Cao, D. In-Situ Growth of Cobalt Oxide Nanoflakes from Cobalt Nanosheet on Nickel Foam for Battery-Type Supercapacitors with High Specific Capacity. *J. Electroanal. Chem.* **2017**, *785*, 103–108. https://doi.org/10.1016/j.jelechem.2016.12.002.

(50) Wang, Y.; Yang, D.; Zhou, T.; Pan, J.; Wei, T.; Sun, Y. Oriented CuCo2S4 Nanograss Arrays/Ni Foam as an Electrode for a High-Performance All-Solid-State Supercapacitor. *Nanotechnology* **2017**, *28* (46). https://doi.org/10.1088/1361-6528/aa8d85.

(51) Kamali-Heidari, E.; Xu, Z. L.; Sohi, M. H.; Ataie, A.; Kim, J. K. Core-Shell Structured Ni3S2 Nanorods Grown on Interconnected Ni-Graphene Foam for Symmetric Supercapacitors. *Electrochim. Acta* **2018**, *271*, 507–518. https://doi.org/10.1016/j.electacta.2018.03.183.

(52) Ali, A.; Ammar, M.; Ali, M.; Yahya, Z.; Javaid, M. Y.; Hassan, S. U.; Ahmed, T. Mo-Doped ZnO Nanoflakes on Ni-Foam for Asymmetric Supercapacitor Applications. *RSC Adv.* **2019**, *9* (47), 27432–27438. https://doi.org/10.1039/c9ra05051e.

(53) Shi, X.; Wang, H.; Ji, S.; Linkov, V.; Liu, F.; Wang, R. CoNiSe2 Nanorods Directly Grown on Ni Foam as Advanced Cathodes for Asymmetric Supercapacitors. *Chem. Eng. J.* **2019**, *364* (December 2018), 320–327. https://doi.org/10.1016/j.cej.2019.01.156.

(54) Zhao, Z.; Shen, T.; Liu, Z.; Zhong, Q.; Qin, Y. Facile Fabrication of Binder-Free Reduced Graphene Oxide/MnO2/Ni Foam Hybrid Electrode for High-Performance Supercapacitors. *J. Alloys Compd.* **2020**, *812*, 152124. https://doi.org/10.1016/j.jallcom.2019.152124.

(55) Wang, R.; Xuan, H.; Zhang, G.; Li, H.; Guan, Y.; Liang, X.; Zhang, S.; Wu, Z.; Han, P.; Wu, Y. Design and Fabrication of Free-Standing Ni3S2/NiV-LDH Nanosheets Arrays on Reduced Graphene Oxide/Ni Foam as a Novel Electrode for Asymmetric

Supercapacitor. *Appl. Surf. Sci.* **2020**, *526*, 146641. https://doi.org/10.1016/j.apsusc.2020.146641.

(56) Meng, Y.; Yu, D.; Teng, Y.; Liu, X.; Liu, X. A High-Performance Electrode Based on the ZnCo2O4@CoMoO4 Core-Shell Nanosheet Arrays on Nickel Foam and Their Application in Battery-Supercapacitor Hybrid Device. *Electrochim. Acta* **2020**, *347*, 136278. https://doi.org/10.1016/j.electacta.2020.136278.

(57) Gopi, C. V. V. M.; Sambasivam, S.; Raghavendra, K. V. G.; Vinodh, R.; Obaidat, I. M.; Kim, H. J. Facile Synthesis of Hierarchical Flower-like NiMoO4-CoMoO4 Nanosheet Arrays on Nickel Foam as an Efficient Electrode for High Rate Hybrid Supercapacitors. *J. Energy Storage* **2020**, *30* (March), 101550. https://doi.org/10.1016/j.est.2020.101550.

(58) Zhao, L.; Lei, S.; Tu, Q.; Rao, L.; Zen, W.; Xiao, Y.; Cheng, B. Phase-Controlled Growth of Nickel Hydroxide Nanostructures on Nickel Foam for Enhanced Supercapacitor Performance. *J. Energy Storage* **2021**, *43* (September), 103171. https://doi.org/10.1016/j.est.2021.103171.

(59) Li, R.; Zhang, W.; Zhang, M.; Peng, Z.; Wang, Y.; Liu, Y.; Zheng, Y.; Guo, X.; Zhang, Y.; Wang, Z.; Zhang, T. High Performance Ni3S2/3D Graphene/Nickel Foam Composite Electrode for Supercapacitor Applications. *Mater. Chem. Phys.* **2021**, *257* (June 2020), 123769. https://doi.org/10.1016/j.matchemphys.2020.123769.

(60) Liu, Z.; Liu, Y.; Zhong, Y.; Cui, L.; Yang, W.; Razal, J. M.; Barrow, C. J.; Liu, J. Facile Construction of MgCo2O4@CoFe Layered Double Hydroxide Core-Shell Nanocomposites on Nickel Foam for High-Performance Asymmetric Supercapacitors. *J. Power Sources* **2021**, *484* (November 2020), 229288. https://doi.org/10.1016/j.jpowsour.2020.229288.

(61) Liu, J.; Han, E.; He, Y.; Tong, X.; Guo, S. Effect of Soft Template on Nickel-Cobalt Layered Double Hydroxides Grown on Nickel Foam as Battery-Type Electrodes for Hybrid Supercapacitors. *Ionics (Kiel).* **2021**, *27* (7), 3129–3141. https://doi.org/10.1007/s11581-021-04050-9.

(62) Zhang, C.; Kuila, T.; Kim, N. H.; Lee, S. H.; Lee, J. H. Facile Preparation of Flower-like NiCo2O4/Three Dimensional Graphene Foam Hybrid for High Performance Supercapacitor Electrodes. *Carbon N. Y.* **2015**, *89*, 328–339. https://doi.org/10.1016/j.carbon.2015.03.051.

(63) Guan, C.; Liu, X.; Ren, W.; Li, X.; Cheng, C.; Wang, J. Rational Design of Metal-Organic Framework Derived Hollow NiCo2O4 Arrays for Flexible Supercapacitor and Electrocatalysis. *Adv. Energy Mater.* **2017**, *7* (12), 1–8. https://doi.org/10.1002/aenm.201602391.

(64) Chatterjee, M.; Kundu, A.; Das, S.; Pradhan, S. K. Ultrastable Asymmetric Supercapacitor Device with Chemically Derived and Mechanically Activated NiCo2O4. *Energy and Fuels* **2022**, *36* (14), 7878–7889. https://doi.org/10.1021/acs.energyfuels.2c01321.

(65) Deokate, R. J.; Kalubarme, R. S.; Park, C. J.; Lokhande, C. D. Simple Synthesis of

NiCo2O4 Thin Films Using Spray Pyrolysis for Electrochemical Supercapacitor Application: A Novel Approach. *Electrochim. Acta* **2017**, *224*, 378–385. https://doi.org/10.1016/j.electacta.2016.12.034.

(66) Gao, J. S.; Liu, Z.; Lin, Y.; Tang, Y.; Lian, T.; He, Y. NiCo2O4 Nanofeathers Derived from Prussian Blue Analogues with Enhanced Electrochemical Performance for Supercapacitor. *Chem. Eng. J.* **2020**, *388* (November 2019), 124368. https://doi.org/10.1016/j.cej.2020.124368.

(67) Wang, N.; Sun, B.; Zhao, P.; Yao, M.; Hu, W.; Komarneni, S. Electrodeposition Preparation of NiCo2O4 Mesoporous Film on Ultrafine Nickel Wire for Flexible Asymmetric Supercapacitors. *Chem. Eng. J.* **2018**, *345* (January), 31–38. https://doi.org/10.1016/j.cej.2018.03.147.

(68) Mordina, B.; Neeraj, N. S.; Srivastava, A. K.; Mukhopadhyay, K.; Prasad, N. E. Investigation of the Structure-Property Relationship in Binder Free Asymmetric Supercapacitor Device Based on NiCo2O4.NH2O Nanostructures. *J. Electroanal. Chem.* **2021**, *880*, 114850. https://doi.org/10.1016/j.jelechem.2020.114850.

(69) Zhang, H.; Xiao, D.; Li, Q.; Ma, Y.; Yuan, S.; Xie, L.; Chen, C.; Lu, C. Porous NiCo2O4 Nanowires Supported on Carbon Cloth for Flexible Asymmetric Supercapacitor with High Energy Density. *J. Energy Chem.* **2018**, *27* (1), 195–202. https://doi.org/10.1016/j.jechem.2017.10.034.

(70) Wang, T.; Guo, Y.; Zhao, B.; Yu, S.; Yang, H. P.; Lu, D.; Fu, X. Z.; Sun, R.; Wong, C. P. NiCo2O4 Nanosheets In-Situ Grown on Three Dimensional Porous Ni Film Current Collectors as Integrated Electrodes for High-Performance Supercapacitors. *J. Power Sources* **2015**, *286*, 371–379. https://doi.org/10.1016/j.jpowsour.2015.03.180.

(71) Zhang, G.; Lou, X. W. General Solution Growth of Mesoporous NiCo2O4 Nanosheets on Various Conductive Substrates as High-Performance Electrodes for Supercapacitors. *Adv. Mater.* **2013**, *25* (7), 976–979. https://doi.org/10.1002/adma.201204128.

(72) Winter, M.; Brodd, R. J. What Are Batteries, Fuel Cells, and Supercapacitors? *Chem. Rev.* **2004**, *104* (10), 4245–4269. https://doi.org/10.1021/cr020730k.

(73) Cheng, F.; Liang, J.; Tao, Z.; Chen, J. Functional Materials for Rechargeable Batteries. *Adv. Mater.* **2011**, *23* (15), 1695–1715. https://doi.org/10.1002/adma.201003587.

(74) Sa, Q.; Wang, Y. Ni Foam as the Current Collector for High Capacity C-Si Composite Electrode. *J. Power Sources* **2012**, *208*, 46–51. https://doi.org/10.1016/j.jpowsour.2012.02.020.

(75) Feng, N.; Hu, D.; Wang, P.; Sun, X.; Li, X.; He, D. Growth of Nanostructured Nickel Sulfide Films on Ni Foam as High-Performance Cathodes for Lithium Ion Batteries. *Phys. Chem. Chem. Phys.* **2013**, *15* (24), 9924–9930. https://doi.org/10.1039/c3cp50615k.

(76) Yang, W.; Cheng, G.; Dong, C.; Bai, Q.; Chen, X.; Peng, Z.; Zhang, Z. NiO Nanorod Array Anchored Ni Foam as a Binder-Free Anode for High-Rate Lithium Ion Batteries. *J. Mater. Chem. A* **2014**, *2* (47), 20022–20029.

https://doi.org/10.1039/c4ta04809a.

(77) Zhao, Q.; Hu, X.; Zhang, K.; Zhang, N.; Hu, Y.; Chen, J. Sulfur Nanodots Electrodeposited on Ni Foam as High-Performance Cathode for Li-S Batteries. *Nano Lett.* **2015**, *15* (1), 721–726. https://doi.org/10.1021/nl504263m.

(78) Zhang, K.; Qin, F.; Fang, J.; Li, Q.; Jia, M.; Lai, Y.; Zhang, Z.; Li, J. Nickel Foam as Interlayer to Improve the Performance of Lithium-Sulfur Battery. *J. Solid State Electrochem.* **2014**, *18* (4), 1025–1029. https://doi.org/10.1007/s10008-013-2351-5.

(79) Wang, L.; Wang, C.; Li, F.; Cheng, F.; Chen, J. In Situ Synthesis of Bi Nanoflakes on Ni Foam for Sodium-Ion Batteries. *Chem. Commun.* **2017**, *54* (1), 38–41. https://doi.org/10.1039/c7cc08341f.

(80) Hu, P.; Wang, T.; Zhao, J.; Zhang, C.; Ma, J.; Du, H.; Wang, X.; Cui, G. Ultrafast Alkaline Ni/Zn Battery Based on Ni-Foam-Supported Ni3S2 Nanosheets. *ACS Appl. Mater. Interfaces* **2015**, *7* (48), 26396–26399. https://doi.org/10.1021/acsami.5b09728.

(81) Chen, Q.; Li, J.; Liao, C.; Hu, G.; Fu, Y.; Asare, O. K.; Shi, S.; Liu, Z.; Zhou, L.; Mai, L. Ni Foam Supported NiO Nanosheets as High-Performance Free-Standing Electrodes for Hybrid Supercapacitors and Ni-Zn Batteries. *J. Mater. Chem. A* **2018**, *6* (40), 19488–19494. https://doi.org/10.1039/c8ta07574c.

(82) Wang, H.; Yu, H.; Yin, S.; Xu, Y.; Li, X.; Xue, H.; Wang, L. Integrated Mesoporous PtPd Film/Ni Foam: An Efficient Binder-Free Cathode for Zn-Air Batteries. *ACS Sustain. Chem. Eng.* **2018**, *6* (9), 12367–12374. https://doi.org/10.1021/acssuschemeng.8b02834.

(83) Ni, S.; Li, T.; Lv, X.; Yang, X.; Zhang, L. Designed Constitution of NiO/Ni Nanostructured Electrode for High Performance Lithium Ion Battery. *Electrochim. Acta* **2013**, *91*, 267–274. https://doi.org/10.1016/j.electacta.2012.12.113.

(84) Wang, J.; Zhang, Q.; Li, X.; Xu, D.; Wang, Z.; Guo, H.; Zhang, K. Three-Dimensional Hierarchical Co3O4/CuO Nanowire Heterostructure Arrays on Nickel Foam for High-Performance Lithium Ion Batteries. *Nano Energy* **2014**, *6*, 19–26. https://doi.org/10.1016/j.nanoen.2014.02.012.

(85) Xiong, L.; Teng, Y.; Wu, Y.; Wang, J.; He, Z. Large-Scale Synthesis of Aligned Co3O4 Nanowalls on Nickel Foam and Their Electrochemical Performance for Li-Ion Batteries. *Ceram. Int.* **2014**, *40* (10), 15561–15568. https://doi.org/10.1016/j.ceramint.2014.07.032.

(86) Chang, J.; Huang, X.; Zhou, G.; Cui, S.; Mao, S.; Chen, J. Three-Dimensional Carbon-Coated Si/RGO Nanostructures Anchored by Nickel Foam with Carbon Nanotubes for Li-Ion Battery Applications. *Nano Energy* **2015**, *15*, 679–687. https://doi.org/10.1016/j.nanoen.2015.05.020.

(87) Tokur, M.; Algul, H.; Uysal, M.; Cetinkaya, T.; Alp, A.; Akbulut, H. Electrolytic Coating of Sn Nano-Rods on Nickel Foam Support for High Performance Lithium Ion Battery Anodes. *Surf. Coatings Technol.* **2016**, *288*, 62–68. https://doi.org/10.1016/j.surfcoat.2016.01.015.

(88) Li, S.; Xie, W.; Gu, L.; Liu, Z.; Hou, X.; Liu, B.; Wang, Q.; He, D. Facilely Scraping Si Nanoparticles@reduced Graphene Oxide Sheets onto Nickel Foam as Binder-Free Electrodes for Lithium Ion Batteries. *Electrochim. Acta* **2016**, *193*, 246–252. https://doi.org/10.1016/j.electacta.2016.02.074.

(89) Mukanova, A.; Nurpeissova, A.; Urazbayev, A.; Kim, S. S.; Myronov, M.; Bakenov, Z. Silicon Thin Film on Graphene Coated Nickel Foam as an Anode for Li-Ion Batteries. *Electrochim. Acta* **2017**, *258*, 800–806. https://doi.org/10.1016/j.electacta.2017.11.129.

(90) Ren, J. T.; Yuan, G. G.; Weng, C. C.; Yuan, Z. Y. Rationally Designed Co3O4-C Nanowire Arrays on Ni Foam Derived from Metal Organic Framework as Reversible Oxygen Evolution Electrodes with Enhanced Performance for Zn-Air Batteries. *ACS Sustain. Chem. Eng.* **2018**, *6* (1), 707–718. https://doi.org/10.1021/acssuschemeng.7b03034.

(91) Xu, K.; Loh, A.; Wang, B.; Li, X. Enhancement of Oxygen Transfer by Design Nickel Foam Electrode for Zinc−Air Battery. *J. Electrochem. Soc.* **2018**, *165* (5), A809–A818. https://doi.org/10.1149/2.0361805jes.

(92) Zhao, H.; Li, D.; Li, H.; Tamirat, A. G.; Song, X.; Zhang, Z.; Wang, Y.; Guo, Z.; Wang, L.; Feng, S. Ru Nanosheet Catalyst Supported by Three-Dimensional Nickel Foam as a Binder-Free Cathode for Li–CO 2 Batteries. *Electrochim. Acta* **2019**, *299*, 592–599. https://doi.org/10.1016/j.electacta.2019.01.027.

(93) Chen, Z.; Zhang, Q.; Lu, L.; Chen, X.; Wang, S.; Xin, C.; Xing, B.; Zhang, C. Enhanced Cycle Stability of Na2Ti3O7 Nanosheets Grown in Situ on Nickel Foam as an Anode for Sodium-Ion Batteries. *Energy and Fuels* **2020**, *34* (3), 3901–3908. https://doi.org/10.1021/acs.energyfuels.9b04307.

(94) Huang, Y.; Li, M.; Chen, S.; Sun, P.; Lv, X.; Li, B.; Fang, L.; Sun, X. Constructing Aqueous Zn//Ni Hybrid Battery with NiSe Nanorod Array on Nickel Foam and Redox Electrolytes for High-Performance Electrochemical Energy Storage. *Appl. Surf. Sci.* **2021**, *562* (May), 150222. https://doi.org/10.1016/j.apsusc.2021.150222.

(95) Chen, D.; Pan, L.; Pei, P.; Huang, S.; Ren, P.; Song, X. Carbon-Coated Oxygen Vacancies-Rich Co3O4 Nanoarrays Grow on Nickel Foam as Efficient Bifunctional Electrocatalysts for Rechargeable Zinc-Air Batteries. *Energy* **2021**, *224*, 120142. https://doi.org/10.1016/j.energy.2021.120142.

(96) Kang, Y.; Wang, S.; Zhu, S.; Gao, H.; Hui, K. S.; Yuan, C. Z.; Yin, H.; Bin, F.; Wu, X. L.; Mai, W.; Zhu, L.; Hu, M.; Liang, F.; Chen, F.; Hui, K. N. Iron-Modulated Nickel Cobalt Phosphide Embedded in Carbon to Boost Power Density of Hybrid Sodium–Air Battery. *Appl. Catal. B Environ.* **2021**, *285* (November 2020), 119786. https://doi.org/10.1016/j.apcatb.2020.119786.

(97) Pakseresht, S.; Cetinkaya, T.; Al-Ogaili, A. W. M.; Halebi, M.; Akbulut, H. Biologically Synthesized TiO2 Nanoparticles and Their Application as Lithium-Air Battery Cathodes. *Ceram. Int.* **2021**, *47* (3), 3994–4005. https://doi.org/10.1016/j.ceramint.2020.09.264.

(98) Cho, G. bong; Kim, J. kwang; Lee, S. hoon; Kim, G. tae; Noh, J. pil; Cho, K. koo; Kim, K. won; Nam, T. hyun; Ahn, H. jun. Facile Fabrication of Patterned Si Film Electrodes Containing Trench-Structured Cu Current Collectors for Thin-Film Batteries. *Electrochim. Acta* **2017**, *224*, 649–659. https://doi.org/10.1016/j.electacta.2016.12.067.

(99) Nam, D. H.; Kim, R. H.; Han, D. W.; Kwon, H. S. Electrochemical Performances of Sn Anode Electrodeposited on Porous Cu Foam for Li-Ion Batteries. *Electrochim. Acta* **2012**, *66*, 126–132. https://doi.org/10.1016/j.electacta.2012.01.084.

(100) Kim, S.-J.; Kim, M.-C.; Han, S.-B.; Lee, G.-H.; Choe, H.-S.; Moon, S.-H.; Kwak, D.-H.; Hong, S.; Park, K.-W. 3-D Si/Carbon Nanofiber as a Binder/Current Collector-Free Anode for Lithium-Ion Batteries. *J. Ind. Eng. Chem.* **2017**, *49*, 105–111. https://doi.org/https://doi.org/10.1016/j.jiec.2017.01.014.

(101) Wang, X.; Sun, L.; Hu, X.; Susantyoko, R. A.; Zhang, Q. Ni–Si Nanosheet Network as High Performance Anode for Li Ion Batteries. *J. Power Sources* **2015**, *280*, 393–396. https://doi.org/https://doi.org/10.1016/j.jpowsour.2015.01.123.

(102) Jing, S.; Jiang, H.; Hu, Y.; Li, C. Directly Grown Si Nanowire Arrays on Cu Foam with a Coral-like Surface for Lithium-Ion Batteries. *Nanoscale* **2014**, *6* (23), 14441–14445. https://doi.org/10.1039/c4nr05469e.

(103) Liu, J.; Zhang, Q.; Zhang, T.; Li, J. T.; Huang, L.; Sun, S. G. A Robust Ion-Conductive Biopolymer as a Binder for Si Anodes of Lithium-Ion Batteries. *Adv. Funct. Mater.* **2015**, *25* (23), 3599–3605. https://doi.org/10.1002/adfm.201500589.

(104) An, Y.; Fei, H.; Zeng, G.; Ci, L.; Xiong, S.; Feng, J.; Qian, Y. Green, Scalable, and Controllable Fabrication of Nanoporous Silicon from Commercial Alloy Precursors for High-Energy Lithium-Ion Batteries. *ACS Nano* **2018**, *12* (5), 4993–5002. https://doi.org/10.1021/acsnano.8b02219.

(105) Li, Z.; Zhang, Y.; Liu, T.; Gao, X.; Li, S.; Ling, M.; Liang, C.; Zheng, J.; Lin, Z. Silicon Anode with High Initial Coulombic Efficiency by Modulated Trifunctional Binder for High-Areal-Capacity Lithium-Ion Batteries. *Adv. Energy Mater.* **2020**, *10* (20), 1–11. https://doi.org/10.1002/aenm.201903110.

(106) Liu, Y.; Huang, K.; Fan, Y.; Zhang, Q.; Sun, F.; Gao, T.; Yang, L.; Zhong, J. Three-Dimensional Network Current Collectors Supported Si Nanowires for Lithium-Ion Battery Applications. *Electrochim. Acta* **2013**, *88*, 766–771. https://doi.org/10.1016/j.electacta.2012.10.129.

(107) Mukanova, A.; Nurpeissova, A.; Kim, S. S.; Myronov, M.; Bakenov, Z. N-Type Doped Silicon Thin Film on a Porous Cu Current Collector as the Negative Electrode for Li-Ion Batteries. *ChemistryOpen* **2018**, *7* (1), 92–96. https://doi.org/10.1002/open.201700162.

(108) Ma, T. Y.; Dai, S.; Jaroniec, M.; Qiao, S. Z. Synthesis of Highly Active and Stable Spinel-Type Oxygen Evolution Electrocatalysts by a Rapid Inorganic Self-Templating Method. *Chem. - A Eur. J.* **2014**, *20* (39), 12669–12676. https://doi.org/10.1002/chem.201403946.

(109) Evans, G. E.; Kordesch, K. V. Hydrazine-Air Fuel Cells. *Science (80-.).* **1967**, *158* (3805), 1148–1152. https://doi.org/10.1126/science.158.3805.1148.

(110) Steele, B. C. H.; Heinzel, A. Materials for Fuel-Cell Technologies. *Nature* **2001**, *414* (6861), 345–352. https://doi.org/10.1038/35104620.

(111) Rajeshkhanna, G.; Ranga Rao, G. Micro and Nano-Architectures of Co3O4 on Ni Foam for Electro-Oxidation of Methanol. *Int. J. Hydrogen Energy* **2018**, *43* (9), 4706–4715. https://doi.org/10.1016/j.ijhydene.2017.10.110.

(112) Wen, H.; Gan, L. Y.; Dai, H. Bin; Wen, X. P.; Wu, L. S.; Wu, H.; Wang, P. In Situ Grown Ni Phosphide Nanowire Array on Ni Foam as a High-Performance Catalyst for Hydrazine Electrooxidation. *Appl. Catal. B Environ.* **2019**, *241* (September 2018), 292–298. https://doi.org/10.1016/j.apcatb.2018.09.043.

(113) Ye, K.; Zhang, H.; Zhao, L.; Huang, X.; Cheng, K.; Wang, G.; Cao, D. Facile Preparation of Three-Dimensional Ni(OH)2/Ni Foam Anode with Low Cost and Its Application in a Direct Urea Fuel Cell. *New J. Chem.* **2016**, *40* (10), 8673–8680. https://doi.org/10.1039/c6nj01648k.

(114) Wang, G.; Ye, K.; Shao, J.; Zhang, Y.; Zhu, K.; Cheng, K.; Yan, J.; Wang, G.; Cao, D. Porous Ni2P Nanoflower Supported on Nickel Foam as an Efficient Three-Dimensional Electrode for Urea Electro-Oxidation in Alkaline Medium. *Int. J. Hydrogen Energy* **2018**, *43* (19), 9316–9325. https://doi.org/10.1016/j.ijhydene.2018.03.221.

(115) Lei, T.; Tian, Y. M.; Wang, G. L.; Yin, J. L.; Gao, Y. Y.; Wen, Q.; Cao, D. X. An Alkaline Al-H2O2 Semi-Fuel Cell Based on a Nickel Foam Supported Co3O4 Nanowire Arrays Cathode. *Fuel Cells* **2011**, *11* (3), 431–435. https://doi.org/10.1002/fuce.201000168.

(116) Liu, X.; Hao, M.; Feng, M.; Zhang, L.; Zhao, Y.; Du, X.; Wang, G. A One-Compartment Direct Glucose Alkaline Fuel Cell with Methyl Viologen as Electron Mediator. *Appl. Energy* **2013**, *106*, 176–183. https://doi.org/10.1016/j.apenergy.2013.01.073.

(117) Cheng, S.; Wu, J. Air-Cathode Preparation with Activated Carbon as Catalyst, PTFE as Binder and Nickel Foam as Current Collector for Microbial Fuel Cells. *Bioelectrochemistry* **2013**, *92*, 22–26. https://doi.org/10.1016/j.bioelechem.2013.03.001.

(118) Tsang, C. H. A.; Hui, K. N.; Hui, K. S.; Ren, L. Deposition of Pd/Graphene Aerogel on Nickel Foam as a Binder-Free Electrode for Direct Electro-Oxidation of Methanol and Ethanol. *J. Mater. Chem. A* **2014**, *2* (42), 17986–17993. https://doi.org/10.1039/c4ta03138e.

(119) Tsang, C. H. A.; Leung, D. Y. C. Pd-Pt Loaded Graphene Aerogel on Nickel Foam Composite as Binder-Free Anode for a Direct Glucose Fuel Cell Unit. *Solid State Sci.* **2017**, *71*, 123–129. https://doi.org/10.1016/j.solidstatesciences.2017.07.014.

(120) Tsang, C. H. A.; Leung, D. Y. C. Use of Pd-Pt Loaded Graphene Aerogel on Nickel Foam in Direct Ethanol Fuel Cell. *Solid State Sci.* **2018**, *75*, 21–26.

https://doi.org/10.1016/j.solidstatesciences.2017.11.005.

(121) Kamyabi, M. A.; Mohammadian, H.; Jadali, S.; Moharramnezhad, M. Hydrothermal Syntheses of NiO−GO Nanocomposite on 3D Nickel Foam as a Support for Pt Nanoparticles and Its Superior Electrocatalytic Activity towards Methanol Oxidation. *Electroanalysis* **2019**, *31* (8), 1501–1510. https://doi.org/10.1002/elan.201800793.

(122) Qian, L.; Luo, S.; Wu, L.; Hu, X.; Chen, W.; Wang, X. In Situ Growth of Metal Organic Frameworks Derived Hierarchical Hollow Porous Co3O4/NiCo2O4 Nanocomposites on Nickel Foam as Self-Supported Flexible Electrode for Methanol Electrocatalytic Oxidation. *Appl. Surf. Sci.* **2020**, *503* (July 2019), 144306. https://doi.org/10.1016/j.apsusc.2019.144306.

(123) Wen, F.; Li, S.; Song, Y.; Sun, L. PdxAuy Loaded Reduced Graphene Oxide on Nickel Foam(PAGN) Composite for High Efficient Methanol and Ethanol Electrooxidation. *Solid State Sci.* **2020**, *110*, 106467. https://doi.org/10.1016/j.solidstatesciences.2020.106467.

(124) Yuan, J.; Zhao, H.; Ouyang, R.; Miao, Y. Ni-Mo Nanorod Bundles Grown within Nickel Foam for Excellent Electrochemical Performance. *Int. J. Electrochem. Sci.* **2020**, *15*, 9579–9589. https://doi.org/10.20964/2020.10.08.

(125) Eisa, T.; Mohamed, H. O.; Choi, Y. J.; Park, S. G.; Ali, R.; Abdelkareem, M. A.; Oh, S. E.; Chae, K. J. Nickel Nanorods over Nickel Foam as Standalone Anode for Direct Alkaline Methanol and Ethanol Fuel Cell. *Int. J. Hydrogen Energy* **2020**, *45* (10), 5948–5959. https://doi.org/10.1016/j.ijhydene.2019.08.071.

(126) Zhang, J.; Leung, P.; Qiao, F.; Xing, L.; Yang, C.; Su, H.; Xu, Q. Balancing the Electron Conduction and Mass Transfer: Effect of Nickel Foam Thickness on the Performance of an Alkaline Direct Ethanol Fuel Cell (ADEFC) with 3D Porous Anode. *Int. J. Hydrogen Energy* **2020**, *45* (38), 19801–19812. https://doi.org/10.1016/j.ijhydene.2020.05.119.

(127) Tang, P. P.; Lin, X.; Yin, H.; Zhang, D. X.; Wen, H.; Wang, J. J.; Wang, P. Hierarchically Nanostructured Nickel-Cobalt Alloy Supported on Nickel Foam as a Highly Efficient Electrocatalyst for Hydrazine Oxidation. *ACS Sustain. Chem. Eng.* **2020**, *8* (44), 16583–16590. https://doi.org/10.1021/acssuschemeng.0c05846.

(128) Liu, R.; Zhou, W.; Li, S.; Li, F.; Ling, W. Performance Improvement of Proton Exchange Membrane Fuel Cells with Compressed Nickel Foam as Flow Field Structure. *Int. J. Hydrogen Energy* **2020**, *45* (35), 17833–17843. https://doi.org/10.1016/j.ijhydene.2020.04.238.

(129) Ćwieka, K.; Lysik, A.; Wejrzanowski, T.; Norby, T.; Xing, W. Microstructure and Electrochemical Behavior of Layered Cathodes for Molten Carbonate Fuel Cell. *J. Power Sources* **2021**, *500* (April), 229949. https://doi.org/10.1016/j.jpowsour.2021.229949.

(130) Dong, X.; Lu, S.; Xu, W.; Li, S. The Fabrication Composite Material of Bimetallic Micro/Nanostructured Palladium-Platinum Alloy and Graphene on Nickel Foam for the Enhancement of Electrocatalytic Activity. *New J. Chem.* **2021**, *45* (14), 6550–

6559. https://doi.org/10.1039/d1nj00196e.

(131) Abdullah, M. I.; Hameed, A.; Zhang, N.; Islam, M. H.; Ma, M.; Pollet, B. G. Ultrasonically Surface-Activated Nickel Foam as a Highly Efficient Monolith Electrode for the Catalytic Oxidation of Methanol to Formate. *ACS Appl. Mater. Interfaces* **2021**, *13* (26), 30603–30613. https://doi.org/10.1021/acsami.1c06258.

(132) Cao, Y.; Ge, J.; Jiang, M.; Zhang, F.; Lei, X. Acid-Etched Co3O4Nanoparticles on Nickel Foam: The Highly Reactive (311) Facet and Enriched Defects for Boosting Methanol Oxidation Electrocatalysis. *ACS Appl. Mater. Interfaces* **2021**, *13* (25), 29491–29499. https://doi.org/10.1021/acsami.1c04045.

(133) Pan, B.; Chen, F.; Wang, J.; Tang, Q.; Guo, L.; Jin, T.; Peng, C.; An, L.; Chen, Y. PdAuAg Alloy Nanoparticles on Nickel Foam as Anode for Passive Air-Breathing Formate Fuel Cell. *J. Electrochem. Soc.* **2021**, *168* (6), 064519. https://doi.org/10.1149/1945-7111/ac0c31.

(134) Wang, L.; Zhang, G.; Liu, Y.; Li, W.; Lu, W.; Huang, H. Facile Synthesis of a Mechanically Robust and Highly Porous NiO Film with Excellent Electrocatalytic Activity towards Methanol Oxidation. *Nanoscale* **2016**, *8* (21), 11256–11263. https://doi.org/10.1039/c6nr01991a.

(135) Jia, Z.; Rondiya, S. R.; Cross, R. W.; Wang, C.; Dzade, N. Y.; Zhang, C. Highly Active Methanol Oxidation Electrocatalyst Based on 2D NiO Porous Nanosheets:A Combined Computational and Experimental Study. *Electrochim. Acta* **2021**, *394*, 139143. https://doi.org/10.1016/j.electacta.2021.139143.

(136) Barakat, N. A. M.; Abdelkareem, M. A.; El-Newehy, M.; Kim, H. Y. Influence of the Nanofibrous Morphology on the Catalytic Activity of NiO Nanostructures: An Effective Impact toward Methanol Electrooxidation. *Nanoscale Res. Lett.* **2013**, *8* (1), 1–6. https://doi.org/10.1186/1556-276X-8-402.

(137) Luo, Q.; Peng, M.; Sun, X.; Asiri, A. M. Hierarchical Nickel Oxide Nanosheet@nanowire Arrays on Nickel Foam: An Efficient 3D Electrode for Methanol Electro-Oxidation. *Catal. Sci. Technol.* **2016**, *6* (4), 1157–1161. https://doi.org/10.1039/c5cy01427a.

(138) Zhang, D.; Zhang, J.; Wang, H.; Cui, C.; Jiao, W.; Gao, J.; Liu, Y. Novel Ni Foam Based Nickel Oxalate Derived Porous NiO Nanostructures as Highly Efficient Electrodes for the Electrooxidation of Methanol/Ethanol and Urea. *J. Alloys Compd.* **2019**, *806*, 1419–1429. https://doi.org/10.1016/j.jallcom.2019.07.127.

(139) Yang, W.; Yang, X.; Jia, J.; Hou, C.; Gao, H.; Mao, Y.; Wang, C.; Lin, J.; Luo, X. Oxygen Vacancies Confined in Ultrathin Nickel Oxide Nanosheets for Enhanced Electrocatalytic Methanol Oxidation. *Appl. Catal. B Environ.* **2019**, *244*, 1096–1102. https://doi.org/https://doi.org/10.1016/j.apcatb.2018.12.038.

(140) Wang, T.-J.; Huang, H.; Wu, X.-R.; Yao, H.-C.; Li, F.-M.; Chen, P.; Jin, P.-J.; Deng, Z.-W.; Chen, Y. Self-Template Synthesis of Defect-Rich NiO Nanotubes as Efficient Electrocatalysts for Methanol Oxidation Reaction. *Nanoscale* **2019**, *11* (42), 19783–19790. https://doi.org/10.1039/C9NR06304H.

(141) Arunachalam, P.; Ghanem, M. A.; Al-Mayouf, A. M.; Al-shalwi, M.; Abd-Elkader, O. H. Microwave Assisted Synthesis and Characterization of Ni/NiO Nanoparticles as Electrocatalyst for Methanol Oxidation in Alkaline Solution. *Mater. Res. Express* **2017**, *4* (2), 025035. https://doi.org/10.1088/2053-1591/aa5ed8.

(142) Xiao, C.; Li, Y.; Lu, X.; Zhao, C. Bifunctional Porous NiFe/NiCo2O4/Ni Foam Electrodes with Triple Hierarchy and Double Synergies for Efficient Whole Cell Water Splitting. *Adv. Funct. Mater.* **2016**, *26* (20), 3515–3523. https://doi.org/10.1002/adfm.201505302.

(143) Wang, H.; Lee, H. W.; Deng, Y.; Lu, Z.; Hsu, P. C.; Liu, Y.; Lin, D.; Cui, Y. Bifunctional Non-Noble Metal Oxide Nanoparticle Electrocatalysts through Lithium-Induced Conversion for Overall Water Splitting. *Nat. Commun.* **2015**, *6*. https://doi.org/10.1038/ncomms8261.

(144) Zhang, X.; Xu, H.; Li, X.; Li, Y.; Yang, T.; Liang, Y. Facile Synthesis of Nickel-Iron/Nanocarbon Hybrids as Advanced Electrocatalysts for Efficient Water Splitting. *ACS Catal.* **2016**, *6* (2), 580–588. https://doi.org/10.1021/acscatal.5b02291.

(145) Toghraei, A.; Shahrabi, T.; Barati Darband, G. Electrodeposition of Self-Supported Ni-Mo-P Film on Ni Foam as an Affordable and High-Performance Electrocatalyst toward Hydrogen Evolution Reaction. *Electrochim. Acta* **2020**, *335*, 135643. https://doi.org/10.1016/j.electacta.2020.135643.

(146) Sivanantham, A.; Ganesan, P.; Shanmugam, S. Hierarchical NiCo2S4 Nanowire Arrays Supported on Ni Foam: An Efficient and Durable Bifunctional Electrocatalyst for Oxygen and Hydrogen Evolution Reactions. *Adv. Funct. Mater.* **2016**, *26* (26), 4661–4672. https://doi.org/10.1002/adfm.201600566.

(147) Kuai, L.; Geng, J.; Chen, C.; Kan, E.; Liu, Y.; Wang, Q.; Geng, B. A Reliable Aerosol-Spray-Assisted Approach to Produce and Optimize Amorphous Metal Oxide Catalysts for Electrochemical Water Splitting. *Angew. Chemie - Int. Ed.* **2014**, *53* (29), 7547–7551. https://doi.org/10.1002/anie.201404208.

(148) Lv, X.; Zhu, Y.; Jiang, H.; Yang, X.; Liu, Y.; Su, Y.; Huang, J.; Yao, Y.; Li, C. Hollow Mesoporous NiCo2O4 Nanocages as Efficient Electrocatalysts for Oxygen Evolution Reaction. *Dalt. Trans.* **2015**, *44* (9), 4148–4154. https://doi.org/10.1039/c4dt03803g.

(149) Zhou, C.; Mu, J.; Qi, Y. F.; Wang, Q.; Zhao, X. J.; Yang, E. C. Iron-Substituted Co-Ni Phosphides Immobilized on Ni Foam as Efficient Self-Supported 3D Hierarchical Electrocatalysts for Oxygen Evolution Reaction. *Int. J. Hydrogen Energy* **2019**, *44* (16), 8156–8165. https://doi.org/10.1016/j.ijhydene.2019.02.053.

(150) Ahn, S. H.; Manthiram, A. Direct Growth of Ternary Ni-Fe-P Porous Nanorods onto Nickel Foam as a Highly Active, Robust Bi-Functional Electrocatalyst for Overall Water Splitting. *J. Mater. Chem. A* **2017**, *5* (6), 2496–2503. https://doi.org/10.1039/c6ta10509b.

(151) Zeng, K.; Zhang, D. Recent Progress in Alkaline Water Electrolysis for Hydrogen Production and Applications. *Prog. Energy Combust. Sci.* **2010**, *36* (3), 307–326.

https://doi.org/10.1016/j.pecs.2009.11.002.

(152) Wang, J.; Cui, W.; Liu, Q.; Xing, Z.; Asiri, A. M.; Sun, X. Recent Progress in Cobalt-Based Heterogeneous Catalysts for Electrochemical Water Splitting. *Adv. Mater.* **2016**, *28* (2), 215–230. https://doi.org/10.1002/adma.201502696.

(153) Liang, Y.; Li, Y.; Wang, H.; Zhou, J.; Wang, J.; Regier, T.; Dai, H. Co3O4 Nanocrystals on Graphene as a Synergistic Catalyst for Oxygen Reduction Reaction. *Nat. Mater.* **2011**, *10* (10), 780–786. https://doi.org/10.1038/nmat3087.

(154) McCrory, C. C. L.; Jung, S.; Peters, J. C.; Jaramillo, T. F. Benchmarking Heterogeneous Electrocatalysts for the Oxygen Evolution Reaction. *J. Am. Chem. Soc.* **2013**, *135* (45), 16977–16987. https://doi.org/10.1021/ja407115p.

(155) Chaudhari, N. K.; Jin, H.; Kim, B.; Lee, K. Nanostructured Materials on 3D Nickel Foam as Electrocatalysts for Water Splitting. *Nanoscale* **2017**, *9* (34), 12231–12247. https://doi.org/10.1039/c7nr04187j.

(156) Xiao, C.; Zhang, B.; Li, D. Partial-Sacrificial-Template Synthesis of Fe/Ni Phosphides on Ni Foam: A Strongly Stabilized and Efficient Catalyst for Electrochemical Water Splitting. *Electrochim. Acta* **2017**, *242*, 260–267. https://doi.org/10.1016/j.electacta.2017.05.015.

(157) Yang, Z.; He, R.; Wu, H.; Ding, Y.; Mei, H. Needle-like CoP/RGO Growth on Nickel Foam as an Efficient Electrocatalyst for Hydrogen Evolution Reaction. *Int. J. Hydrogen Energy* **2021**, *46* (15), 9690–9698. https://doi.org/10.1016/j.ijhydene.2020.07.114.

(158) Lado, J. L.; Wang, X.; Paz, E.; Carbó-Argibay, E.; Guldris, N.; Rodríguez-Abreu, C.; Liu, L.; Kovnir, K.; Kolenko, Y. V. Design and Synthesis of Highly Active Al-Ni-P Foam Electrode for Hydrogen Evolution Reaction. *ACS Catal.* **2015**, *5* (11), 6503–6508. https://doi.org/10.1021/acscatal.5b01761.

(159) Bai, N.; Li, Q.; Mao, D.; Li, D.; Dong, H. One-Step Electrodeposition of Co/CoP Film on Ni Foam for Efficient Hydrogen Evolution in Alkaline Solution. *ACS Appl. Mater. Interfaces* **2016**, *8* (43), 29400–29407. https://doi.org/10.1021/acsami.6b07785.

(160) Zhou, W.; Wu, X. J.; Cao, X.; Huang, X.; Tan, C.; Tian, J.; Liu, H.; Wang, J.; Zhang, H. Ni3S2 Nanorods/Ni Foam Composite Electrode with Low Overpotential for Electrocatalytic Oxygen Evolution. *Energy Environ. Sci.* **2013**, *6* (10), 2921–2924. https://doi.org/10.1039/c3ee41572d.

(161) Liang, Y.; Sun, X.; Asiri, A. M.; He, Y. Amorphous Ni-B Alloy Nanoparticle Film on Ni Foam: Rapid Alternately Dipping Deposition for Efficient Overall Water Splitting. *Nanotechnology* **2016**, *27* (12). https://doi.org/10.1088/0957-4484/27/12/12LT01.

(162) Cao, J.; Zhou, J.; Zhang, Y.; Wang, Y.; Liu, X. Dominating Role of Aligned MoS2/Ni3S2 Nanoarrays Supported on Three-Dimensional Ni Foam with Hydrophilic Interface for Highly Enhanced Hydrogen Evolution Reaction. *ACS Appl. Mater. Interfaces* **2018**, *10* (2), 1752–1760. https://doi.org/10.1021/acsami.7b16407.

(163) Yang, L.; Guo, Z.; Huang, J.; Xi, Y.; Gao, R.; Su, G.; Wang, W.; Cao, L.; Dong, B.

Vertical Growth of 2D Amorphous FePO4 Nanosheet on Ni Foam: Outer and Inner Structural Design for Superior Water Splitting. *Adv. Mater.* **2017**, *29* (46), 1–9. https://doi.org/10.1002/adma.201704574.

(164) Yan, K. L.; Shang, X.; Li, Z.; Dong, B.; Chi, J. Q.; Liu, Y. R.; Gao, W. K.; Chai, Y. M.; Liu, C. G. Facile Synthesis of Binary NiCoS Nanorods Supported on Nickel Foam as Efficient Electrocatalysts for Oxygen Evolution Reaction. *Int. J. Hydrogen Energy* **2017**, *42* (27), 17129–17135. https://doi.org/10.1016/j.ijhydene.2017.05.235.

(165) Kou, T.; Wang, S.; Hauser, J. L.; Chen, M.; Oliver, S. R. J.; Ye, Y.; Guo, J.; Li, Y. Ni Foam-Supported Fe-Doped β-Ni(OH) 2 Nanosheets Show Ultralow Overpotential for Oxygen Evolution Reaction. *ACS Energy Lett.* **2019**, *4* (3), 622–628. https://doi.org/10.1021/acsenergylett.9b00047.

(166) Niu, S.; Sun, Y.; Sun, G.; Rakov, D.; Li, Y.; Ma, Y.; Chu, J.; Xu, P. Stepwise Electrochemical Construction of FeOOH/Ni(OH)2 on Ni Foam for Enhanced Electrocatalytic Oxygen Evolution. *ACS Appl. Energy Mater.* **2019**, *2* (5), 3927–3935. https://doi.org/10.1021/acsaem.9b00785.

(167) Gao, Y.; He, H.; Tan, W.; Peng, Y.; Dai, X.; Wu, Y. One-Step Potentiostatic Electrodeposition of Ni–Se–Mo Film on Ni Foam for Alkaline Hydrogen Evolution Reaction. *Int. J. Hydrogen Energy* **2020**, *45* (11), 6015–6023. https://doi.org/10.1016/j.ijhydene.2019.12.163.

(168) Liang, C.; Cao, W.; Zhou, L.; Yang, P.; Zhao, X.; Zhao, P.; Qiu, R.; Yang, L.; Huang, Q. song; Astruc, D. Design, Synthesis and High HER Performances of 3D Ni/Mo Sulfide on Ni Foam. *ChemCatChem* **2020**, *12* (6), 1647–1652. https://doi.org/10.1002/cctc.201902278.

(169) Li, J.; Xu, W.; Luo, J.; Zhou, D.; Zhang, D.; Wei, L.; Xu, P.; Yuan, D. Synthesis of 3d Hexagram-like Cobalt–Manganese Sulfides Nanosheets Grown on Nickel Foam: A Bifunctional Electrocatalyst for Overall Water Splitting. *Nano-Micro Lett.* **2018**, *10* (1), 1–10. https://doi.org/10.1007/s40820-017-0160-6.

(170) Yan, K. L.; Qin, J. F.; Liu, Z. Z.; Dong, B.; Chi, J. Q.; Gao, W. K.; Lin, J. H.; Chai, Y. M.; Liu, C. G. Organic-Inorganic Hybrids-Directed Ternary NiFeMoS Anemone-like Nanorods with Scaly Surface Supported on Nickel Foam for Efficient Overall Water Splitting. *Chem. Eng. J.* **2018**, *334* (October 2017), 922–931. https://doi.org/10.1016/j.cej.2017.10.074.

(171) Song, G.; Wang, Z.; Sun, J.; Sun, J.; Yuan, D.; Zhang, L. ZnCo2S4 Nanosheet Array Anchored on Nickel Foam as Electrocatalyst for Electrochemical Water Splitting. *Electrochem. commun.* **2019**, *105* (May), 106487. https://doi.org/10.1016/j.elecom.2019.106487.

(172) Wang, W.; Yang, Z.; Jiao, F.; Gong, Y. (P, W)-Codoped MoO2 Nanoflowers on Nickel Foam as an Efficient Bifunctional Electrocatalyst for Overall Water Splitting. *Appl. Surf. Sci.* **2020**, *529* (April). https://doi.org/10.1016/j.apsusc.2020.146987.

(173) Xue, H.; Meng, A.; Zhang, H.; Lin, Y.; Li, Z.; Wang, C. 3D Urchin like V-Doped CoP in Situ Grown on Nickel Foam as Bifunctional Electrocatalyst for Efficient Overall

Water-Splitting. *Nano Res.* **2021**, *12* (1). https://doi.org/10.1007/s12274-021-3359-2.

(174) Zhang, C.; Du, X.; Wang, Y.; Han, X.; Zhang, X. NiSe2@NixSy Nanorod on Nickel Foam as Efficient Bifunctional Electrocatalyst for Overall Water Splitting. *Int. J. Hydrogen Energy* **2021**, *46* (70), 34713–34726. https://doi.org/10.1016/j.ijhydene.2021.08.046.

(175) Wu, X.; Li, J.; Li, Y.; Wen, Z. NiFeP-MoO2 Hybrid Nanorods on Nickel Foam as High-Activity and High-Stability Electrode for Overall Water Splitting. *Chem. Eng. J.* **2021**, *409* (October 2020), 128161. https://doi.org/10.1016/j.cej.2020.128161.

(176) Dong, J.; Zhang, F. Q.; Yang, Y.; Zhang, Y. B.; He, H.; Huang, X.; Fan, X.; Zhang, X. M. (003)-Facet-Exposed Ni3S2 Nanoporous Thin Films on Nickel Foil for Efficient Water Splitting. *Appl. Catal. B Environ.* **2019**, *243*, 693–702. https://doi.org/10.1016/j.apcatb.2018.11.003.

(177) Yang, C.; Gao, M. Y.; Zhang, Q. B.; Zeng, J. R.; Li, X. T.; Abbott, A. P. In-Situ Activation of Self-Supported 3D Hierarchically Porous Ni3S2 Films Grown on Nanoporous Copper as Excellent PH-Universal Electrocatalysts for Hydrogen Evolution Reaction. *Nano Energy* **2017**, *36*, 85–94. https://doi.org/10.1016/j.nanoen.2017.04.032.

(178) Lin, T. W.; Liu, C. J.; Dai, C. S. Ni3S2/Carbon Nanotube Nanocomposite as Electrode Material for Hydrogen Evolution Reaction in Alkaline Electrolyte and Enzyme-Free Glucose Detection. *Appl. Catal. B Environ.* **2014**, *154–155*, 213–220. https://doi.org/10.1016/j.apcatb.2014.02.017.

(179) Cui, K.; Fan, J.; Li, S.; Li, S.; Fatiya Khadidja, M.; Wu, J.; Wang, M.; Lai, J.; Jin, H.-G.; Luo, W.; Chao, Z. Facile Synthesis and Electrochemical Performances of Three Dimensional Ni3S2 as Bifunctional Electrode for Overall Water Splitting. *Mater. Sci. Eng. B* **2021**, *263*, 114875. https://doi.org/https://doi.org/10.1016/j.mseb.2020.114875.

(180) Ho, T. A.; Bae, C.; Nam, H.; Kim, E.; Lee, S. Y.; Park, J. H.; Shin, H. Metallic Ni3S2 Films Grown by Atomic Layer Deposition as an Efficient and Stable Electrocatalyst for Overall Water Splitting. *ACS Appl. Mater. Interfaces* **2018**, *10* (15), 12807–12815. https://doi.org/10.1021/acsami.8b00813.

(181) Li, J.; Shen, P. K.; Tian, Z. One-Step Synthesis of Ni3S2 Nanowires at Low Temperature as Efficient Electrocatalyst for Hydrogen Evolution Reaction. *Int. J. Hydrogen Energy* **2017**, *42* (10), 7136–7142. https://doi.org/10.1016/j.ijhydene.2016.03.068.

(182) Yao, M.; Sun, B.; He, L.; Wang, N.; Hu, W.; Komarneni, S. Self-Assembled Ni 3 S 2 Nanosheets with Mesoporous Structure Tightly Held on Ni Foam as a Highly Efficient and Long-Term Electrocatalyst for Water Oxidation. *ACS Sustain. Chem. Eng.* **2019**, *7* (5), 5430–5439. https://doi.org/10.1021/acssuschemeng.8b06525.

(183) Shi, J.; Hu, J.; Luo, Y.; Sun, X.; Asiri, A. M. Ni3Se2 Film as a Non-Precious Metal Bifunctional Electrocatalyst for Efficient Water Splitting. *Catal. Sci. Technol.* **2015**, *5* (11), 4954–4958. https://doi.org/10.1039/c5cy01121c.

(184) Crouch, E.; Cowell, D. C.; Hoskins, S.; Pittson, R. W.; Hart, J. P. A Novel,

Disposable, Screen-Printed Amperometric Biosensor for Glucose in Serum Fabricated Using a Water-Based Carbon Ink. *Biosens. Bioelectron.* **2005**, *21* (5), 712–718. https://doi.org/10.1016/j.bios.2005.01.003.

(185) Bahadir, E. B.; Sezgintürk, M. K. Applications of Commercial Biosensors in Clinical, Food, Environmental, and Biothreat/Biowarfare Analyses. *Analytical Biochemistry*. 2015, pp 107–120. https://doi.org/10.1016/j.ab.2015.03.011.

(186) Yuan, J.; Wang, K.; Xia, X. Highly Ordered Platinum-Nanotubule Arrays for Amperometric Glucose Sensing. *Adv. Funct. Mater.* **2005**, *15* (5), 803–809. https://doi.org/10.1002/adfm.200400321.

(187) Oliver, N. S.; Toumazou, C.; Cass, A. E. G.; Johnston, D. G. Glucose Sensors: A Review of Current and Emerging Technology. *Diabetic Medicine*. 2009, pp 197–210. https://doi.org/10.1111/j.1464-5491.2008.02642.x.

(188) Shul'ga, A. A.; Soldatkin, A. P.; El'skaya, A. V.; Dzyadevich, S. V.; Patskovsky, S. V.; Strikha, V. I. Thin-Film Conductometric Biosensors for Glucose and Urea Determination. *Biosens. Bioelectron.* **1994**, *9* (3), 217–223. https://doi.org/10.1016/0956-5663(94)80124-X.

(189) Nakayama, D.; Takeoka, Y.; Watanabe, M.; Kataoka, K. Simple and Precise Preparation of a Porous Gel for a Colorimetric Glucose Sensor by a Templating Technique. *Angew. Chemie* **2003**, *115* (35), 4329–4332. https://doi.org/10.1002/ange.200351746.

(190) Pickup, J. C.; Hussain, F.; Evans, N. D.; Rolinski, O. J.; Birch, D. J. S. Fluorescence-Based Glucose Sensors. *Biosensors and Bioelectronics*. 2005, pp 2555–2565. https://doi.org/10.1016/j.bios.2004.10.002.

(191) Li, Y.; He, X.; Guo, M.; Lin, D.; Xu, C.; Xie, F.; Sun, X. Porous NiTe2 Nanosheet Array: An Effective Electrochemical Sensor for Glucose Detection. *Sensors Actuators, B Chem.* **2018**, *274*, 427–432. https://doi.org/10.1016/j.snb.2018.07.172.

(192) Song, Y.; Qu, K.; Zhao, C.; Ren, J.; Qu, X. Graphene Oxide: Intrinsic Peroxidase Catalytic Activity and Its Application to Glucose Detection. *Adv. Mater.* **2010**, *22* (19), 2206–2210. https://doi.org/10.1002/adma.200903783.

(193) Xia, C.; Ning, W. A Novel Non-Enzymatic Electrochemical Glucose Sensor Modified with FeOOH Nanowire. *Electrochem. commun.* **2010**, *12* (11), 1581–1584. https://doi.org/10.1016/j.elecom.2010.09.002.

(194) Wu, S.; Zeng, Z.; He, Q.; Wang, Z.; Wang, S. J.; Du, Y.; Yin, Z.; Sun, X.; Chen, W.; Zhang, H. Electrochemically Reduced Single-Layer MoS2 Nanosheets: Characterization, Properties, and Sensing Applications. *Small* **2012**, *8* (14), 2264–2270. https://doi.org/10.1002/smll.201200044.

(195) Shoji, E.; Freund, M. Synthesis and Electrochemical Properties of Poly (Aniline Boronic Acid): A Novel Transduction Method for a Non-Enzymatic Glucose Sensor and a Precursor Route. *J. Am. Chem. Soc* **2001**, No. December.

(196) Zhuang, Z.; Su, X.; Yuan, H.; Sun, Q.; Xiao, D.; Choi, M. M. F. An Improved

Sensitivity Non-Enzymatic Glucose Sensor Based on a CuO Nanowire Modified Cu Electrode. *Analyst* **2008**, *133* (1), 126–132. https://doi.org/10.1039/b712970j.

(197) Wu, H. X.; Cao, W. M.; Li, Y.; Liu, G.; Wen, Y.; Yang, H. F.; Yang, S. P. In Situ Growth of Copper Nanoparticles on Multiwalled Carbon Nanotubes and Their Application as Non-Enzymatic Glucose Sensor Materials. *Electrochim. Acta* **2010**, *55* (11), 3734–3740. https://doi.org/10.1016/j.electacta.2010.02.017.

(198) Park, S.; Boo, H.; Chung, T. D. Electrochemical Non-Enzymatic Glucose Sensors. *Analytica Chimica Acta*. 2006, pp 46–57. https://doi.org/10.1016/j.aca.2005.05.080.

(199) Xu, H.; Xia, C.; Wang, S.; Han, F.; Akbari, M. K.; Hai, Z.; Zhuiykov, S. Electrochemical Non-Enzymatic Glucose Sensor Based on Hierarchical 3D Co3O4/Ni Heterostructure Electrode for Pushing Sensitivity Boundary to a New Limit. *Sensors Actuators, B Chem.* **2018**, *267*, 93–103. https://doi.org/10.1016/j.snb.2018.04.023.

(200) Toghill, K. E.; Compton, R. G. Electrochemical Non-Enzymatic Glucose Sensors: A Perspective and an Evaluation. *Int. J. Electrochem. Sci.* **2010**, *5* (9), 1246–1301.

(201) Nie, H.; Yao, Z.; Zhou, X.; Yang, Z.; Huang, S. Nonenzymatic Electrochemical Detection of Glucose Using Well-Distributed Nickel Nanoparticles on Straight Multi-Walled Carbon Nanotubes. *Biosens. Bioelectron.* **2011**, *30* (1), 28–34. https://doi.org/10.1016/j.bios.2011.08.022.

(202) Mu, Y.; Jia, D.; He, Y.; Miao, Y.; Wu, H. L. Nano Nickel Oxide Modified Non-Enzymatic Glucose Sensors with Enhanced Sensitivity through an Electrochemical Process Strategy at High Potential. *Biosens. Bioelectron.* **2011**, *26* (6), 2948–2952. https://doi.org/10.1016/j.bios.2010.11.042.

(203) Lu, W.; Qin, X.; Asiri, A. M.; Al-Youbi, A. O.; Sun, X. Ni Foam: A Novel Three-Dimensional Porous Sensing Platform for Sensitive and Selective Nonenzymatic Glucose Detection. *Analyst* **2013**, *138* (2), 417–420. https://doi.org/10.1039/c2an36138h.

(204) Chandrasekaran, N. I.; Manickam, M. A Sensitive and Selective Non-Enzymatic Glucose Sensor with Hollow Ni-Al-Mn Layered Triple Hydroxide Nanocomposites Modified Ni Foam. *Sensors Actuators, B Chem.* **2019**, *288* (August 2018), 188–194. https://doi.org/10.1016/j.snb.2019.02.102.

(205) Guo, C.; Wang, Y.; Zhao, Y.; Xu, C. Non-Enzymatic Glucose Sensor Based on Three Dimensional Nickel Oxide for Enhanced Sensitivity. *Anal. Methods* **2013**, *5* (7), 1644–1647. https://doi.org/10.1039/c3ay00067b.

(206) Kung, C. W.; Cheng, Y. H.; Ho, K. C. Single Layer of Nickel Hydroxide Nanoparticles Covered on a Porous Ni Foam and Its Application for Highly Sensitive Non-Enzymatic Glucose Sensor. *Sensors Actuators, B Chem.* **2014**, *204*, 159–166. https://doi.org/10.1016/j.snb.2014.07.102.

(207) Huo, H.; Zhao, Y.; Xu, C. 3D Ni3S2 Nanosheet Arrays Supported on Ni Foam for High-Performance Supercapacitor and Non-Enzymatic Glucose Detection. *J. Mater. Chem. A* **2014**, *2* (36), 15111–15117. https://doi.org/10.1039/c4ta02857k.

(208) Zhao, Y.; Gu, G.; You, S.; Ji, R.; Suo, H.; Zhao, C.; Liu, F. Preparation of Ni(OH)2 Nanosheets on Ni Foam via a Direct Precipitation Method for a Highly Sensitive Non-Enzymatic Glucose Sensor. *RSC Adv.* **2015**, *5* (66), 53665–53670. https://doi.org/10.1039/c5ra06664f.

(209) Wang, L.; Xie, Y.; Wei, C.; Lu, X.; Li, X.; Song, Y. Hierarchical NiO Superstructures/Foam Ni Electrode Derived from Ni Metal-Organic Framework Flakes on Foam Ni for Glucose Sensing. *Electrochim. Acta* **2015**, *174*, 846–852. https://doi.org/10.1016/j.electacta.2015.06.086.

(210) Zhao, B.; Wang, T.; Jiang, L.; Zhang, K.; Yuen, M. M. F.; Xu, J. Bin; Fu, X. Z.; Sun, R.; Wong, C. P. NiO Mesoporous Nanowalls Grown on RGO Coated Nickel Foam as High Performance Electrodes for Supercapacitors and Biosensors. *Electrochim. Acta* **2016**, *192*, 205–215. https://doi.org/10.1016/j.electacta.2016.01.211.

(211) Zhang, L.; Ding, Y.; Li, R.; Ye, C.; Zhao, G.; Wang, Y. Ni-Based Metal-Organic Framework Derived Ni@C Nanosheets on a Ni Foam Substrate as a Supersensitive Non-Enzymatic Glucose Sensor. *J. Mater. Chem. B* **2017**, *5* (28), 5549–5555. https://doi.org/10.1039/c7tb01363a.

(212) Lu, Y.; Jiang, B.; Fang, L.; Fan, S.; Wu, F.; Hu, B.; Meng, F. M. Highly Sensitive Nonenzymatic Glucose Sensor Based on 3D Ultrathin NiFe Layered Double Hydroxide Nanosheets. *Electroanalysis* **2017**, *29* (7), 1755–1761. https://doi.org/10.1002/elan.201700025.

(213) Xia, K.; Yang, C.; Chen, Y.; Tian, L.; Su, Y.; Wang, J.; Li, L. In Situ Fabrication of Ni(OH)2 Flakes on Ni Foam through Electrochemical Corrosion as High Sensitive and Stable Binder-Free Electrode for Glucose Sensing. *Sensors Actuators, B Chem.* **2017**, *240*, 979–987. https://doi.org/10.1016/j.snb.2016.09.077.

(214) Dai, H.; Cao, P.; Chen, D.; Li, Y.; Wang, N.; Ma, H.; Lin, M. Ni-Co-S/PPy Core-Shell Nanohybrid on Nickel Foam as a Non-Enzymatic Electrochemical Glucose Sensor. *Synth. Met.* **2018**, *235* (November 2017), 97–102. https://doi.org/10.1016/j.synthmet.2017.12.004.

(215) Guo, Q.; Zeng, W.; Li, Y. Highly Sensitive Non-Enzymatic Glucose Sensor Based on Porous NiCo2O4 Nanowires Grown on Nickel Foam. *Mater. Lett.* **2019**, *256*, 126603. https://doi.org/10.1016/j.matlet.2019.126603.

(216) Hayat, A.; Mane, S. K. B.; Shaishta, N.; Khan, J.; Hayat, A.; Keyum, G.; Uddin, I.; Raziq, F.; Khan, M.; Manjunatha, G. Nickel Oxide Nano-Particles on 3D Nickel Foam Substrate as a Non-Enzymatic Glucose Sensor. *J. Electrochem. Soc.* **2019**, *166* (15), B1602–B1611. https://doi.org/10.1149/2.0491915jes.

(217) Liu, S.; Zeng, W.; Li, Y. Synthesis of ZnCo2O4 Microrods Grown on Nickel Foam for Non-Enzymatic Glucose Sensing. *Mater. Lett.* **2020**, *259*, 126820. https://doi.org/10.1016/j.matlet.2019.126820.

(218) Farid, A.; Pan, L.; Usman, M.; Khan, I. A.; Khan, A. S.; Ahmad, A. ul; Javid, M. In-Situ Growth of Porous CoTe2 Nanosheets Array on 3D Nickel Foam for Highly Sensitive Binder-Free Non-Enzymatic Glucose Sensor. *J. Alloys Compd.* **2021**, *861*,

158642. https://doi.org/10.1016/j.jallcom.2021.158642.

(219) Jeong, H.; Kwac, L. K.; Hong, C. G.; Kim, H. G. Direct Growth of Flower Like-Structured CuFe Oxide on Graphene Supported Nickel Foam as an Effective Sensor for Glucose Determination. *Mater. Sci. Eng. C* **2021**, *118* (April 2020), 111510. https://doi.org/10.1016/j.msec.2020.111510.

(220) Wang, C.; Han, B.; Li, J.; Gao, Q.; Xia, K.; Zhou, C. Direct Epitaxial Growth of Nickel Phosphide Nanosheets on Nickel Foam as Self-Support Electrode for Efficient Non-Enzymatic Glucose Sensing. *Nanotechnology* **2021**, *32* (43). https://doi.org/10.1088/1361-6528/ac162f.

(221) Li, X.; Lu, X.; Kan, X.; Li, X.; Lu, X.; Kan, X. 3D Electrochemical Sensor Based on Poly(Hydroquinone)/Gold Nanoparticles/Nickel Foam for Dopamine Sensitive Detection. *J. Electroanal. Chem.* **2017**, *799* (June), 451–458. https://doi.org/10.1016/j.jelechem.2017.06.047.

(222) Soomro, R. A.; Ibupoto, Z. H.; Sirajuddin; Abro, M. I.; Willander, M. Electrochemical Sensing of Glucose Based on Novel Hedgehog-like NiO Nanostructures. *Sensors Actuators, B Chem.* **2015**, *209*, 966–974. https://doi.org/10.1016/j.snb.2014.12.050.

(223) He, G.; Tian, L.; Cai, Y.; Wu, S.; Su, Y.; Yan, H.; Pu, W.; Zhang, J.; Li, L. Sensitive Nonenzymatic Electrochemical Glucose Detection Based on Hollow Porous NiO. *Nanoscale Res. Lett.* **2018**, *13* (1), 3. https://doi.org/10.1186/s11671-017-2406-0.

(224) Zhang, C.; Qian, L.; Zhang, K.; Yuan, S.; Xiao, J.; Wang, S. Hierarchical Porous Ni/NiO Core-Shells with Superior Conductivity for Electrochemical Pseudo-Capacitors and Glucose Sensors. *J. Mater. Chem. A* **2015**, *3* (19), 10519–10525. https://doi.org/10.1039/c5ta01071c.

(225) Garcia-Garcia, F. J.; Salazar, P.; Yubero, F.; González-Elipe, A. R. Non-Enzymataic Glucose Electrochemical Sensor Made of Porous NiO Thin Films Prepared by Reactive Magnetron Sputtering at Oblique Angles. *Electrochim. Acta* **2016**, *201*, 38–44. https://doi.org/10.1016/j.electacta.2016.03.193.

(226) Ahmad, R.; Khan, M.; Tripathy, N.; Khan, M. I. R.; Khosla, A. Hydrothermally Synthesized Nickel Oxide Nanosheets for Non-Enzymatic Electrochemical Glucose Detection. *J. Electrochem. Soc.* **2020**, *167* (10), 107504. https://doi.org/10.1149/1945-7111/ab9757.

(227) Singer, N.; Pillai, R. G.; Johnson, A. I. D.; Harris, K. D.; Jemere, A. B. Nanostructured Nickel Oxide Electrodes for Non-Enzymatic Electrochemical Glucose Sensing. *Microchim. Acta* **2020**, *187* (4), 196. https://doi.org/10.1007/s00604-020-4171-5.

(228) Gu, J.; Xu, Y.; Li, Q.; Pang, H. Porous Ni/NiO Nanohybrids for Electrochemical Catalytic Glucose Oxidation. *Chinese Chem. Lett.* **2021**, *32* (6), 2017–2020. https://doi.org/10.1016/j.cclet.2020.11.066.

(229) Wang, S.; Wang, C.; Wei, G.; Xiao, H.; An, N.; Zhou, Y.; An, C.; Zhang, J. Non-Enzymatic Glucose Sensor Based on Facial Hydrothermal Synthesized NiO Nanosheets Loaded on Glassy Carbon Electrode. *Colloids Surfaces A Physicochem. Eng. Asp.* **2016**, *509*, 252–258. https://doi.org/10.1016/j.colsurfa.2016.08.076.

(230) Zhang, L.; Liu, J.; Peng, X.; Cui, Q.; He, D.; Zhao, C.; Suo, H. Fabrication of a Ni Foam-Supported Platinum Nanoparticles-Silver/Polypyrrole Electrode for Aqueous Ammonia Sensing. *Synth. Met.* **2020**, *259* (November 2019), 116257. https://doi.org/10.1016/j.synthmet.2019.116257.

(231) Moreira, F. C.; Boaventura, R. A. R.; Brillas, E.; Vilar, V. J. P. Electrochemical Advanced Oxidation Processes: A Review on Their Application to Synthetic and Real Wastewaters. *Appl. Catal. B Environ.* **2017**, *202*, 217–261. https://doi.org/10.1016/j.apcatb.2016.08.037.

(232) Zhang, Y.; Zhang, Q.; Zuo, S.; Zhou, M.; Pan, Y.; Ren, G.; Li, Y.; Zhang, Y. A Highly Efficient Flow-through Electro-Fenton System Enhanced with Nitrilotriacetic Acid for Phenol Removal at Neutral PH. *Sci. Total Environ.* **2019**, *697*, 134173. https://doi.org/10.1016/j.scitotenv.2019.134173.

(233) Zhang, T.; Wang, Y.; Hu, Y.; Wang, Z.; Chen, J.; Niu, X.; Li, Y.; Gong, X. HO[Rad] Selective Cleavage Fe[Sbnd]S Bond for FeS 2 Electrolysis in Alkaline Solution. *Electrochim. Acta* **2019**, *306*, 327–338. https://doi.org/10.1016/j.electacta.2019.03.114.

(234) Deng, F.; Olvera-Vargas, H.; Garcia-Rodriguez, O.; Qiu, S.; Ma, F.; Chen, Z.; Lefebvre, O. Unconventional Electro-Fenton Process Operating at a Wide PH Range with Ni Foam Cathode and Tripolyphosphate Electrolyte. *J. Hazard. Mater.* **2020**, *396* (April), 122641. https://doi.org/10.1016/j.jhazmat.2020.122641.

(235) Pignatello, J. J.; Oliveros, E.; MacKay, A. Advanced Oxidation Processes for Organic Contaminant Destruction Based on the Fenton Reaction and Related Chemistry. *Crit. Rev. Environ. Sci. Technol.* **2006**, *36* (1), 1–84. https://doi.org/10.1080/10643380500326564.

(236) Nidheesh, P. V.; Gandhimathi, R. Trends in Electro-Fenton Process for Water and Wastewater Treatment: An Overview. *Desalination* **2012**, *299*, 1–15. https://doi.org/10.1016/j.desal.2012.05.011.

(237) Sirés, I.; Brillas, E.; Oturan, M. A.; Rodrigo, M. A.; Panizza, M. Electrochemical Advanced Oxidation Processes: Today and Tomorrow. A Review. *Environ. Sci. Pollut. Res.* **2014**, *21* (14), 8336–8367. https://doi.org/10.1007/s11356-014-2783-1.

(238) Hassan, M.; Olvera-Vargas, H.; Zhu, X.; Zhang, B.; He, Y. Microbial Electro-Fenton: An Emerging and Energy-Efficient Platform for Environmental Remediation. *J. Power Sources* **2019**, *424* (March), 220–244. https://doi.org/10.1016/j.jpowsour.2019.03.112.

(239) Mohn, W. W.; Tiedje, J. M. Microbial Reductive Dehalogenation. *Microbiological Reviews*. 1992, pp 482–507. https://doi.org/10.1128/mmbr.56.3.482-507.1992.

(240) Cao, Z.; Liu, X.; Xu, J.; Zhang, J.; Yang, Y.; Zhou, J.; Xu, X.; Lowry, G. V. Removal of Antibiotic Florfenicol by Sulfide-Modified Nanoscale Zero-Valent Iron. *Environ. Sci. Technol.* **2017**, *51* (19), 11269–11277. https://doi.org/10.1021/acs.est.7b02480.

(241) Han, Y.; Liu, C.; Horita, J.; Yan, W. Trichloroethene Hydrodechlorination by Pd-Fe Bimetallic Nanoparticles: Solute-Induced Catalyst Deactivation Analyzed by Carbon Isotope Fractionation. *Appl. Catal. B Environ.* **2016**, *188*, 77–86. https://doi.org/10.1016/j.apcatb.2016.01.047.

(242) Kopinke, F. D.; Speichert, G.; Mackenzie, K.; Hey-Hawkins, E. Reductive Dechlorination in Water: Interplay of Sorption and Reactivity. *Appl. Catal. B Environ.* **2016**, *181*, 747–753. https://doi.org/10.1016/j.apcatb.2015.08.031.

(243) Liu, X.; Cao, Z.; Yuan, Z.; Zhang, J.; Guo, X.; Yang, Y.; He, F.; Zhao, Y.; Xu, J. Insight into the Kinetics and Mechanism of Removal of Aqueous Chlorinated Nitroaromatic Antibiotic Chloramphenicol by Nanoscale Zero-Valent Iron. *Chem. Eng. J.* **2018**, *334* (June 2017), 508–518. https://doi.org/10.1016/j.cej.2017.10.060.

(244) Mao, X.; Ciblak, A.; Baek, K.; Amiri, M.; Loch-Caruso, R.; Alshawabkeh, A. N. Optimization of Electrochemical Dechlorination of Trichloroethylene in Reducing Electrolytes. *Water Res.* **2012**, *46* (6), 1847–1857. https://doi.org/10.1016/j.watres.2012.01.002.

(245) Song, S.; Su, Y.; Adeleye, A. S.; Zhang, Y.; Zhou, X. Optimal Design and Characterization of Sulfide-Modified Nanoscale Zerovalent Iron for Diclofenac Removal. *Appl. Catal. B Environ.* **2017**, *201*, 211–220. https://doi.org/10.1016/j.apcatb.2016.07.055.

(246) Payne, K. A. P.; Quezada, C. P.; Fisher, K.; Dunstan, M. S.; Collins, F. A.; Sjuts, H.; Levy, C.; Hay, S.; Rigby, S. E. J.; Leys, D. Reductive Dehalogenase Structure Suggests a Mechanism for B12-Dependent Dehalogenation. *Nature* **2015**, *517* (7535), 513–516. https://doi.org/10.1038/nature13901.

(247) Li, Y.; Li, X.; Sun, Y.; Zhao, X.; Li, Y. Cathodic Microbial Community Adaptation to the Removal of Chlorinated Herbicide in Soil Microbial Fuel Cells. *Environ. Sci. Pollut. Res.* **2018**, *25* (17), 16900–16912. https://doi.org/10.1007/s11356-018-1871-z.

(248) Xu, Y.; Gregory, K. B.; VanBriesen, J. M. Microbial-Catalyzed Reductive Dechlorination of Polychlorinated Biphenyls in Hudson and Grasse River Sediment Microcosms: Determination of Dechlorination Preferences and Identification of Rare Ortho Removal Pathways. *Environ. Sci. Technol.* **2016**, *50* (23), 12767–12778. https://doi.org/10.1021/acs.est.6b03892.

(249) Agarwal, S.; Al-Abed, S. R.; Dionysiou, D. D. Impact of Organic Solvents and Common Anions on 2-Chlorobiphenyl Dechlorination Kinetics with Pd/Mg. *Appl. Catal. B Environ.* **2009**, *92* (1–2), 17–22. https://doi.org/10.1016/j.apcatb.2009.07.029.

(250) Liu, Y.; Phenrat, T.; Lowry, G. V. Effect of TCE Concentration and Dissolved Groundwater Solutes on NZVI-Promoted TCE Dechlorination and H2 Evolution. *Environ. Sci. Technol.* **2007**, *41* (22), 7881–7887. https://doi.org/10.1021/es0711967.

(251) Zhou, J.; Han, Y.; Wang, W.; Xu, Z.; Wan, H.; Yin, D.; Zheng, S.; Zhu, D. Reductive Removal of Chloroacetic Acids by Catalytic Hydrodechlorination over Pd/ZrO2 Catalysts. *Appl. Catal. B Environ.* **2013**, *134–135*, 222–230. https://doi.org/10.1016/j.apcatb.2013.01.005.

(252) Hozalski, R. M.; Zhang, L.; Arnold, W. A. Reduction of Haloacetic Acids by Fe0: Implications for Treatment and Fate. *Environ. Sci. Technol.* **2001**, *35* (11), 2258–2263. https://doi.org/10.1021/es001785b.

(253) Li, D.; Mao, Z.; Zhong, Y.; Huang, W.; Wu, Y.; Peng, P. Reductive Transformation of

Tetrabromobisphenol A by Sulfidated Nano Zerovalent Iron. *Water Res.* **2016**, *103*, 1–9. https://doi.org/10.1016/j.watres.2016.07.003.

(254) Zhao, B.; Li, X.; Li, W.; Yang, L.; Li, J.; Xia, W.; Zhou, L.; Wang, F.; Zhao, C. Degradation of Trichloroacetic Acid by an Efficient Fenton/UV/TiO2 Hybrid Process and Investigation of Synergetic Effect. *Chem. Eng. J.* **2015**, *273*, 527–533. https://doi.org/10.1016/j.cej.2015.03.012.

(255) Martin, E. T.; McGuire, C. M.; Mubarak, M. S.; Peters, D. G. Electroreductive Remediation of Halogenated Environmental Pollutants. *Chem. Rev.* **2016**, *116* (24), 15198–15234. https://doi.org/10.1021/acs.chemrev.6b00531.

(256) Cheng, I. F.; Fernando, Q.; Korte, N. Electrochemical Dechlorination of 4-Chlorophenol to Phenol. *Environ. Sci. Technol.* **1997**, *31* (4), 1074–1078. https://doi.org/10.1021/es960602b.

(257) Radjenović, J.; Farré, M. J.; Mu, Y.; Gernjak, W.; Keller, J. Reductive Electrochemical Remediation of Emerging and Regulated Disinfection Byproducts. *Water Res.* **2012**, *46* (6), 1705–1714. https://doi.org/10.1016/j.watres.2011.12.042.

(258) Yang, B.; Yu, G.; Huang, J. Electrocatalytic Hydrodechlorination of 2,4,5-Trichlorobiphenyl on a Palladium-Modified Nickel Foam Cathode. *Environ. Sci. Technol.* **2007**, *41* (21), 7503–7508. https://doi.org/10.1021/es071168o.

(259) Lee, J. Y.; Lee, J. G.; Lee, S. H.; Seo, M.; Piao, L.; Bae, J. H.; Lim, S. Y.; Park, Y. J.; Chung, T. D. Hydrogen-Atom-Mediated Electrochemistry. *Nat. Commun.* **2013**, *4* (May), 1–8. https://doi.org/10.1038/ncomms3766.

(260) Li, A.; Zhao, X.; Hou, Y.; Liu, H.; Wu, L.; Qu, J. The Electrocatalytic Dechlorination of Chloroacetic Acids at Electrodeposited Pd/Fe-Modified Carbon Paper Electrode. *Appl. Catal. B Environ.* **2012**, *111–112*, 628–635. https://doi.org/10.1016/j.apcatb.2011.11.016.

(261) Sun, C.; Baig, S. A.; Lou, Z.; Zhu, J.; Wang, Z.; Li, X.; Wu, J.; Zhang, Y.; Xu, X. Electrocatalytic Dechlorination of 2,4-Dichlorophenoxyacetic Acid Using Nanosized Titanium Nitride Doped Palladium/Nickel Foam Electrodes in Aqueous Solutions. *Appl. Catal. B Environ.* **2014**, *158–159*, 38–47. https://doi.org/10.1016/j.apcatb.2014.04.004.

(262) Xie, W.; Yuan, S.; Mao, X.; Hu, W.; Liao, P.; Tong, M.; Alshawabkeh, A. N. Electrocatalytic Activity of Pd-Loaded Ti/TiO2 Nanotubes Cathode for TCE Reduction in Groundwater. *Water Res.* **2013**, *47* (11), 3573–3582. https://doi.org/10.1016/j.watres.2013.04.004.

(263) Yang, L.; Chen, Z.; Cui, D.; Luo, X.; Liang, B.; Yang, L.; Liu, T.; Wang, A.; Luo, S. Ultrafine Palladium Nanoparticles Supported on 3D Self-Supported Ni Foam for Cathodic Dechlorination of Florfenicol. *Chem. Eng. J.* **2019**, *359* (August 2018), 894–901. https://doi.org/10.1016/j.cej.2018.11.099.

(264) Lou, Z.; Zhou, J.; Sun, M.; Xu, J.; Yang, K.; Lv, D.; Zhao, Y.; Xu, X. MnO2 Enhances Electrocatalytic Hydrodechlorination by Pd/Ni Foam Electrodes and Reduces Pd Needs. *Chem. Eng. J.* **2018**, *352* (July), 549–557.

https://doi.org/10.1016/j.cej.2018.07.057.

(265) Guo, C.; Ran, J.; Vasileff, A.; Qiao, S. Z. Rational Design of Electrocatalysts and Photo(Electro)Catalysts for Nitrogen Reduction to Ammonia (NH3) under Ambient Conditions. *Energy Environ. Sci.* **2018**, *11* (1), 45–56. https://doi.org/10.1039/c7ee02220d.

(266) Cui, X.; Tang, C.; Zhang, Q. A Review of Electrocatalytic Reduction of Dinitrogen to Ammonia under Ambient Conditions. *Adv. Energy Mater.* **2018**, *8* (22), 1–25. https://doi.org/10.1002/aenm.201800369.

(267) Marnellos, G.; Stoukides, M. Ammonia Synthesis at Atmospheric Pressure. *Science (80-.).* **1998**, *282* (5386), 98–100. https://doi.org/10.1126/science.282.5386.98.

(268) Ren, X.; Zhao, J.; Wei, Q.; Ma, Y.; Guo, H.; Liu, Q.; Wang, Y.; Cui, G.; Asiri, A. M.; Li, B.; Tang, B.; Sun, X. High-Performance N 2 -to-NH 3 Conversion Electrocatalyzed by Mo 2 C Nanorod. *ACS Cent. Sci.* **2019**, *5* (1), 116–121. https://doi.org/10.1021/acscentsci.8b00734.

(269) Li, Y.; Yu, H.; Wang, Z.; Liu, S.; Xu, Y.; Li, X.; Wang, L.; Wang, H. Boron-Doped Silver Nanosponges with Enhanced Performance towards Electrocatalytic Nitrogen Reduction to Ammonia. *Chem. Commun.* **2019**, *55* (98), 14745–14748. https://doi.org/10.1039/c9cc07232b.

(270) Li, X.; Ren, X.; Liu, X.; Zhao, J.; Sun, X.; Zhang, Y.; Kuang, X.; Yan, T.; Wei, Q.; Wu, D. A MoS 2 Nanosheet-Reduced Graphene Oxide Hybrid: An Efficient Electrocatalyst for Electrocatalytic N 2 Reduction to NH 3 under Ambient Conditions. *J. Mater. Chem. A* **2019**, *7* (6), 2524–2528. https://doi.org/10.1039/c8ta10433f.

(271) Zhang, R.; Ren, X.; Shi, X.; Xie, F.; Zheng, B.; Guo, X.; Sun, X. Enabling Effective Electrocatalytic N2 Conversion to NH3 by the TiO2 Nanosheets Array under Ambient Conditions. *ACS Appl. Mater. Interfaces* **2018**, *10* (34), 28251–28255. https://doi.org/10.1021/acsami.8b06647.

(272) Wang, Z.; Li, Y.; Yu, H.; Xu, Y.; Xue, H.; Li, X.; Wang, H.; Wang, L. Ambient Electrochemical Synthesis of Ammonia from Nitrogen and Water Catalyzed by Flower-Like Gold Microstructures. *ChemSusChem* **2018**, *11* (19), 3480–3485. https://doi.org/10.1002/cssc.201801444.

(273) Wang, H.; Yu, H.; Wang, Z.; Li, Y.; Xu, Y.; Li, X.; Xue, H.; Wang, L. Electrochemical Fabrication of Porous Au Film on Ni Foam for Nitrogen Reduction to Ammonia. *Small* **2019**, *15* (6), 1–7. https://doi.org/10.1002/smll.201804769.

(274) Yu, H.; Wang, Z.; Yin, S.; Li, C.; Xu, Y.; Li, X.; Wang, L.; Wang, H. Mesoporous Au3Pd Film on Ni Foam: A Self-Supported Electrocatalyst for Efficient Synthesis of Ammonia. *ACS Appl. Mater. Interfaces* **2020**, *12* (1), 436–442. https://doi.org/10.1021/acsami.9b14187.

(275) Wang, Z.; Dai, Z.; Yu, H.; Zhang, H.; Tian, W.; Xu, Y.; Li, X.; Wang, L.; Wang, H. Pore-Size-Tuned Pd Films Grown on Ni Foam as an Advanced Catalyst for Electrosynthesis of Ammonia. *ACS Sustain. Chem. Eng.* **2020**, *8* (31), 11827–11833. https://doi.org/10.1021/acssuschemeng.0c04295.

(276) Li, Y.; Yu, H.; Wang, Z.; Liu, S.; Xu, Y.; Li, X.; Wang, L.; Wang, H. One-Step Synthesis of Self-Standing Porous Palladium-Ruthenium Nanosheet Array on Ni Foam for Ambient Electrosynthesis of Ammonia. *Int. J. Hydrogen Energy* **2020**, *45* (11), 5997–6005. https://doi.org/10.1016/j.ijhydene.2019.12.098.